RADIATION SHIELDING CALCULATIONS BY MEANS OF MCNPX

by

France Mbongeni Lukhele

A thesis submitted in partial fulfilment of the requirements
for the degree of Master of Science
in the Department of Physics and Engineering,
University of Zululand

Supervisors:
Supervisor: Prof. O.M Ndwandwe
Co-supervisor: Dr. E. Z. Buthelezi

January 2006

DECLARATION

I, the undersigned, declare that the work contained in this thesis is my own original work and has not previously in its entirety or in part been submitted at any university for a degree.

Signature: ..... **Date:** 2006/04/13

To my late mum, Maria

RADIATION SHIELDING CALCULATIONS BY MEANS OF MCNPX

ABSTRACT

Monte Carlo radiation transport calculations were performed to re-evaluate the configuartion of the horizontal target bombardment station of the radionuclide production at iThemba LABS. Calculated neutron and photon dose attenuation factors for this shield were compared with those previously obtained by means of the multigroup discrete ordinate code. Isotropic and anisotropic source terms were assumed. Furthermore, two geometries were considered, namely, spherical and cylindrical

The neutron and photon total dose rates and dose attenuation factors were calculated at 1.5 m from the center of the target for a shield configuration composed of a combination of homogeneous materials such as iron, paraffin wax containing boron carbide for the attenuation of neutrons, and lastly, lead as an outer photon shield layer. The thickness of lead necessary to attenuate photons transmitted from the neutron capture reactions and those from the decay of the residual nuclei was about 4 cm. The amount of boron carbide needed to mix with paraffin wax was determined by adding, by weight percent, small increments of boron carbide into paraffin wax until about 10% of the boron carbide was eventually added into the wax. The thickness of iron and wax needed to attenuate fast neutrons to thermal neutrons was determined by fixing the total thickness of the shield 60 cm and the position of iron, with respect to iron/wax interface was determined by moving iron across the shield configuration. Where available, the results obtained by means of MCNPX were compared with those previously published.

ACKNOWLEGMENTS

I wish to express my gratitude to the following people without them this project would not have been possible.

- God through his only son, the Lord Jesus Christ for making it possible for my research to be completed.
- My supervisor, Dr. E. Z. Buthelezi, for her invaluable supervision and encouragement that lead to the completion of my project research.
- Mr T. J. van Rooyen for his support with the Radiation Protection.
- Prof. O. M. Ndwandwe and the late T. K. Marais for allowing me to be part of MANUS/MATSI programme.
- My mentor, Danie Moller for his advices and unmeasurable support.
- My colleague, Tebogo Kupi, for support and believing that I can do it and challeging me.
- My father, Sizwe, Nonkululeko, Thulani, Sylvia, Wanda and Lindiwe for their love sacrifice and encouragement through the tenure of my studies.
- Siyakudumisa Dyushu, Xolani Mncedane, Charles Tobo, Lindiwe Mhlauli, Evans Hlatshwayo and Grant Sedres for their friendship, support assistance they have provided at some stage during the project.
- Friends, Family and colleagues whom I have not mentioned, but who are in my heart.
- The personnel of Radioisotope Production Group of iThemba LABS.

Contents

List of Tables

List of Figures

Chapter 1

INTRODUCTION

1.1 Overview

iThemba LABS is a multidisciplinary research facility that provides basic and applied research using particle beams, neutron and proton radiotherapy for the treatment of cancer and for supplying cyclotron-produced radioisotopes for applications in nuclear medicine, industry and research. The main accelerator, the seperated-sector cyclotron (SSC), accelerates protons up to 200 MeV and heavier charge particles to much higher energies. The accelerated particles are then steered to different areas of the facility e.g. radiotherapy vaults, isotope production, etc. The layout of the facility is given in Figure 1.1.

There are four beamlines available for the production of radionuclides at iThemba LABS. Three of these beamlines are horizontal and are all located in one vault while the vertical bemline is located in a separate vault. All these beamlines branch from the SSC to the radionuclide group vaults (see Figure 1.1). Two of the three beamlines were built in 1988 and have been

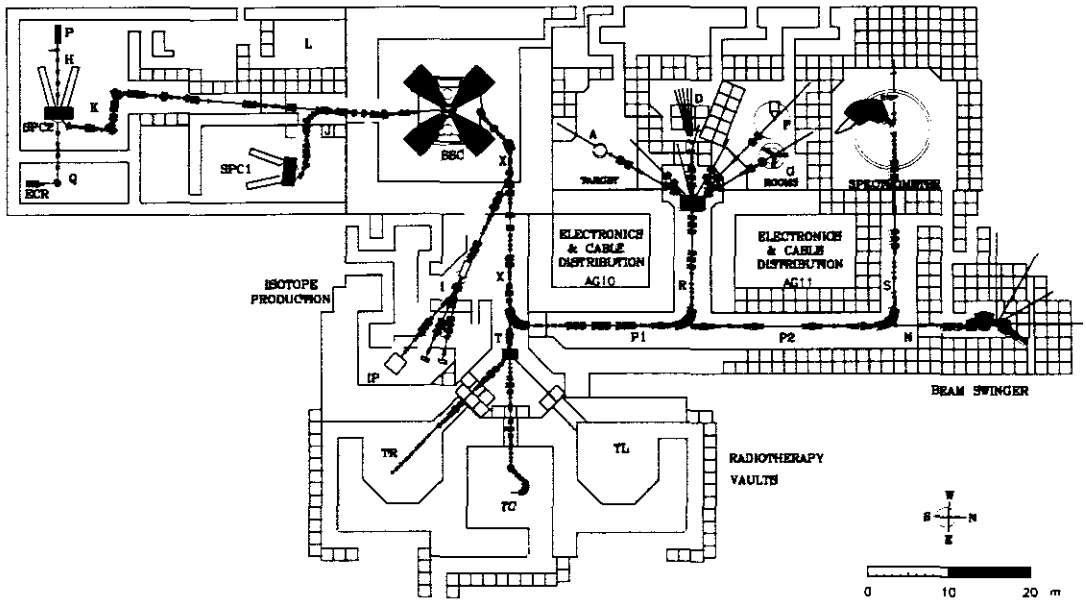

Figure 1.1: A layout of the experimental facilities at iThemba LABS

in operation ever since. The other beamline is reserved for furture developments. One beamline is utilized for high-energy and low current experiments ($\pm$100 MeV, currents up to $\pm$100 nA) employing stacked-foil activation techniques. The other horizontal beamline, so called "elephant" is dedicated to the routine production of radionuclides, [Ste90], [Nor90]. Radionuclides and radiopharmaceuticals are produced routinely at iThemba LABS. These are then supplied to local and international communities.

1.2 Motivation

The "elephant" is a sophisticated, remote-controlled target bombardment station used for the routine production of radionuclides produced by irradiating various targets with 66 MeV proton beams at currents up to 100 μA. Three targets can be irradiated in tandem in this target bombardment station. The "elephant" is located in a vault that has 4.5 m thick concrete walls for biological shielding of neutrons and gamma radiations. In the design of such a bombardment station it is essential to take into account radiation damage to materials inside the vaults. Considerable radiation damage to materials and components of organic nature e.g. rubbers, plastics, etc. can occur in a relatively short period of time. And, because it is impractical to totally exclude radiation from bombardment vaults it is therefore ideal and safer to limit the amount of radiation levels in these areas. In this way personnel are not exposed to unnecessary radiations.In addition, not only is it impractical to replace components of the bombardment station on regular basis it is costly as well. For this reason the bombardment station should be designed in such a way that the target is enclosed inside a suitable local radiation shield and sensitive components mounted outside the shield. In this way the components are prevented from excessive radiation damage and, at the same time, the shield serves to reduce neutron activation of the vaults and its contents.

At iThemba the the vertical beam target station is still under development and its current set-up is such that it is open at the top and is not completely closed at the bottom hence it is not very clear where the neutrons and photons and their associated dose rates are going, especially in position where the equipment is mounted. It is therefore essential to do an investigation

of the neutron and photon dose rates in this vaults and, also on the areas above and below the vault where the vertical beam target station (VBTS) is situated. Such a study was previously conducted by Steyn et al [Ste90, Ste92] whereby dosimetry experiments were performed. The experimental data, together with radiation transport calculations help desgn the shield of the "elephant". These radiation transport calculation were performed by means of the multigroup discrete ordinate code, which is based on the deterministic method. With this code only isotropic source terms could be model. Over the years the use of deterministic-type code have been over-shadowed by the Monte Carlo based codes such as FLUKA at INFN [Fas01], GEANT4 at CERN [CER05] can also be downloaded freely, MCNP/MCNPX at LANL [MCN05] because of their various applications. Although the deterministic codes are still used for simple-geometry problems they are however not as dynamic as Monte Carlo codes, such that the multigroup discrete ordinate codes are almost absolete. Due to their versatility Monte Carlo codes are generally very big. As such one needs to have a good understanding of their capabilities. Since MCNPX is available at iThemba LABS it was therefore chosen as a tool to perform the radiation transport calculations. However, since this code has never been used for this purpose at iThemba LABS it was then decided to test it by re-modeling the shielding of the "elephant" and then compare those results with those obtained by Steyn et al. in 1992 [Ste92]. The results from these calculations would be used as benchmark for the radiation shielding calculations of the VBTS.

1.3 Radiation transport codes

For many decades scientific research was based on the physical experiments, as a basic for developing and refining theory. This however changed with the discovery of numerical experiments. Now scientific theories can be based on numerical experiments that are compared with physical experiments. Numerical experiments provide more information and better understanding of the physical phenomena. The analysis of the results of numerical experiments can guide the selection and the design of the physical experiments best suited to valid theories [AMC94]. The numerical experiments are based on computational techniques i.e. the transportation of neutral particles, which is described by the linear Boltzmann transport equation. It is well known that the Boltzmann equation is mathematically complex hence it cannot be solved analytically. There are several accurate computer codes that can approximate the solution to the Boltzmann transport equation. These codes are available from the Radiation Shielding Information Center (RSIC) at Oak Ridge National Laboratory [RSI05]). Numerical modeling is based on two general approaches viz. deterministic methods and Monte Carlo technique.

The Deterministic method is based on the discrete ordinate and function expansion. It is a numerical technique for solving the finite-difference form of the Boltzmann transport equation. It involves solutions of an integral and differential equation that describes the dependence on a spatial coordinates or time of some behavioural characteristics of the system in question. In other words it is characterized by the functions that describe the phase space density of a particle at a given point and its distributions with respect to energy, angle and particle type. The Boltzmann transport equation is set in an approximate form that allows the calculation of the increment

change in the characteristic caused by an incremental change in the variable(s). Depending on the boundary conditions (for a given source) the equations of flux, heating, reaction rates, etc. are directly solved. Deterministic codes such as RAMA [Bak99], CENTRM [Wil95], ANISN [Eng73], DOT 3.5 [Rho73] compute the neutron flux spectra in one dimensional system or infinite homogeneous media. They also solve the multigroup intergral transport equation using the method of characteristics in arbitral 3-dimensional geometry.The are two areas that limits accurracy in deterministics codes compared to continuous-energy Monte Carlo codes, namely, improved geometrical modeling and utilization of pointwise nuclear data [Wil99].

Monte Carlo method is a numerical technique that allows the calculation of the deterministic quality as an average of the corresponding stochastic one over its probability distribution. It is also called stochastic method. It is eminently suitable for study of stochastic processes, particularly, the motion of excited nucleons such as photons and neutrons inside the nucleus where the nucleus is treated as a Fermi gas after the nucleon-nucleon interaction. It generates statistical random numbers to decide on the entry point of the incident particle in the nucleus, the energy and the direction of the incident particle. The transportation of the emitted radiations i.e. photons and neutrons is characterized by the particles traveling along a straight path between a space of collision points. If a collision occurred the particle may be absorbed or scattered into a new direction and energy. The calculated nucleons are those that are excited by means of intranuclear cascade and emitted when they reach the nuclear surface. This proccess is terminated when the nucleus cannot emit particles anymore. The remaining energy in the nucleus is assumed to be statistically distributed among all nucleons, with the formation

of a fully equilibrated residual nucleus which further decays by evaporation [Hod97]. As a result of this simulation the flux density is obtained by averaging the scores from individual tracks.

Monte Carlo codes e.g. MCNP [Bri93] have been available for years but they were not considered for most practical routine calculations. Contrary, deterministic codes were used based on approximate methods for reactor physics and shielding calculations. Various theoretical models are implemented in Monte Carlo codes to describe the stages of the interactions. The interaction are described by the first stage, pre-equilibrium, evaporation/fission, and lastly de-excitation of residual nucleus. At high incident energies (MeV) the interactions are described by the intranuclear interaction cascade while the transition between the first reaction and final equilibrium is described by the pre-equilibrium and evaporation models. There are various approaches used to describe the pre-equilibrium phase e.g. quantum mechanical multistep model, exciton model, hybrid model and geometry-dependent hybrid models. The intranuclear cascade model is successful in describing the main features of proton-nucleus reactions. This model also provides a good description of the first stage of reaction processes characterised by nucleon-nucleon reaction scatterings and predicts, satisfactorily, the high energy part of the particle spectra. The intranuclear cascade model started in classical multiple scattering by Serber [Ser47]. Later on other aspects such as nuclear mean field, Pauli blocking and the stochastic determination of the final state in binary collisions were introduced. In some models, quantum effects of Paul blocking are taken into account, however using this feature usually adds considerably to the computational time.

Two approaches are commonly used in the pre-equilibrium model, namely multistep model and exciton model. The multistep reaction theory is embodied by three main theories e.g. Feshback, Kerman and Koonin (FKK) [Fes80, Fes95], Tamura, Udagawa and Lenske [TUL] [Tam82] and Nishioka, Weidenmuller and Yoshida (NWY) [Nis88]. In this case the evolution of the reaction proceeds through definite steps from the initial nucleon-nucleon interaction (first step), with each successive step driving the reaction towards the formation of the compound nucleus. The pre-equilibrium exciton model Gi66] and hybrid model are based on the notion of an exciton i.e. particle above or hole below the Fermi level. The initial stage of the reaction of the projectile and the nucleus is responsible for the essential part of emission at high-energy end of the spectrum. The initial number of degrees of freedom in exciton or hybrid model plays an important role. Over the years models were developed [Bla75] to reproduce the pre-equilibrium cross sections and describe the reaction process in terms of a series of nucleon-nucleon interaction within the nucleus. The pre-equilibrium exciton model is governed by the set of master equations which describes both competing processes, the equilibration of the nucleus and the emission. Because of the simplicity and physical transparency of this model, the exciton model continues to be used in spite of the development of more microscopic and quantum mechanical models.

1.4 Objectives

In this study the radiation shield is designed by performing radiation transport calculations by means of MCNPX. Previously, these calculations were performed by employing the multigroup discrete ordinate code. Due to lim-

itation of the multigroup discrete code, which were eluded to in section 1.2 above, only isotropic source terms could be modeled [Ste92]. There are two main objectives of this study:

- To reproduce the data obtained by Steyn *et al.* using the multigroup discrete ordinate code.
- To model anisotropic source terms and compare the results with those obtained using isotropic source terms.

Chapter 2

THEORETICAL BACKGROUND

2.1 Overview

When the target material is irradiated with a beam of charged particles many different interactions occur between the particles and the target nuclei. Some of these interactions are relevant in the production of radionuclides and also in the development and maintenance of the target bombardment station. As such an understanding of fundamental processes is required in order to limit or control the problems inherent in the production of radionuclides. Furthermore, it is equally important to understand the processes by which the charged particles lose their energy in matter. These processes include stopping power of charge particles, energy and range straggling, small-angle multiple scattering and non-elastic nuclear reactions. This chapter provides a detailed description of these processes.

2.2 Passage of charge particles in matter

Heavy charged particles are defined as energetic ions with mass of one atomic mass unit or greater, e.g. protons, alphas, products of many nuclear reactions, fission products, etc. The passage of a charged particle through matter is characterized by two principal features which arise from collisions with atomic electrons of the target material and elastic scattering from nuclei. The two principal features are:

- the practical continuous loss of energy by the particles leading to well-defined ranges, and
- the deflection of the particles from their original direction of movement

A charged particle being surrounded by its Coulomb electric field interacts with every atom of matter it passes. Upon entering the target the particle immediately interacts simultaneously with many electrons, which results with an electron feeling an impulse from the attractive Coulomb force as the particle passes its vicinity. Depending on the proximity of the encounter the electron can either be *excited* to a higher-lying shell within the target or it can be *ionized* by being completely removed from the atom. Only minute fractions of the kinetic energy of the projectile are transfered from most of these interactions. Subsequently, the particle suffers small deviations from its original direction of movement. Due to these encounters the velocity of the projectile is also decreased and because the kinetic energy transfered from the projectile to the target nucleons is so small, it loses its kinetic energy in many such interactions during its passage. Since the interactions are with many electrons the net effect is to decrease the velocity of the particle continuously until it is stopped.

The electronic collisions are generally characterized into groups of *soft* or *hard* collisions. *Soft* collisions take place at distances considerably larger than the atomic radius and the influence of the projectile's Coulomb field affects the atom as a whole, resulting in the *excitation* or *ionization* of electrons. *Hard* collisions happens when the projectile hits the atom and interacts, more likely, with a single atomic electron which is then ejected from the atom as a delta ray (δ - ray) with a considerable kinetic energy. At close encounters the Coulomb interaction occurs with the atomic nucleus as well. In this case the projectile is scattered elastically and the amount of kinetic energy lost by the projectile is just enough to satisfy conservation of momentum. The energy transfered from the charged particle to the target material is ultimately dissipated into molecular vibrations or heat.

2.2.1 Energy loss and stopping power

The stopping power, S, for charged particles is defined as the particle energy loss per unit thickness as it traverses the target material [Jan82]. It is frequently refered to as the "rate of change of energy", S=-dE/dx. The stopping power is an important quantity for calculating the heat deposited by the projectile in the target and also, for calculating the range of the particles as well as their energy at a particular depth in the target material. Since the energy loss of the charge particle is caused primarily by inelastic Coulomb field interactions with the bound atomic electrons of the target material then the projectile disperses a small fraction of its energy in every resulting atomic excitation, ionization or single electron collision. Because the number of interaction per unit path length is very large the resulting effect is a considerable cumulative energy loss occuring in thin layers of the target

material. The energy loss resulting from both these processes is defined a

$$-\frac{dE}{dx} = \frac{4\pi e^4 z^2 Z^2}{mv^2}[ln(\frac{mv^2}{I}) + ln(\frac{1}{1-\beta^2}) - \beta^2 - \frac{C}{Z}], \tag{2.1}$$

where, the parameter I and C/Z represent the mean ionization potential of the target atom and shell correction, respectively. The parameter $\beta = v/c$, is related to the kinetic energy of the particle, c and v represent the particle velocity and velocity of light, repsectively. The electron charge is denoted by e while m represents the electron mass. The atomic numbers of the particle and target are respectively presented by z and Z .

In MCNPX the ionization potentials have been enhanced to the values and enterpolation procedure recommended by the International Commission on Radiation Units and Measurements [ICR84] thereby bringing the model into closer ICRU compliance. To correct for the density effects the parameterization of Sternheimer and Peierls [Ste71] are used. In the case of high energy protons and other light charged particles the full kinetic energy transfer is implemented.

2.2.2 Pathlength

The pathlength is defined as the average distance travelled by a beam of particles from the point where it enters the target material with a specific kinetic energy to the point at which the kinetic energy is equal to zero. It includes track deflections caused by angular scattering and is sometimes referd to as the "continuous slowing down approximation range". The range, R, is defined as the average depth of penetration of charge particles measured

along a straight line parrallel to the original direction of the motion of the particles. The relation of range to energy loss is given as

$$R = \int_0^{E_0} (\frac{dE}{dx})^{-1} dE \tag{2.2}$$

where E_0 is the energy of the projectile and $-dE/dx$ is the stopping power for the projectile in a target material. The range is always less than the path-length because of angular deflection caused by multiple scattering processes. Figure 2.1 gives a rough illustration of the pathlength and range of protons within a target material.

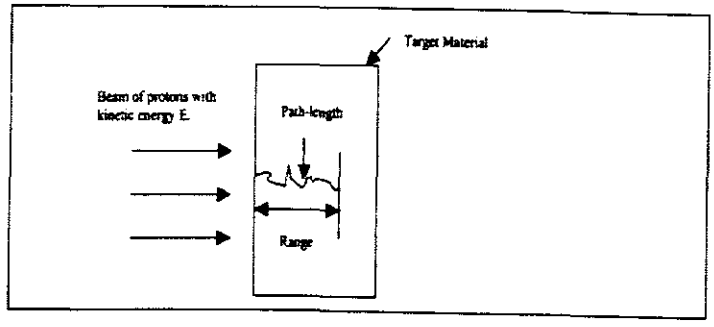

Figure 2.1: Schematic representation of the pathlength and range of particles in the target material.

2.2.3 Energy and range straggling

The energy lost by a projectile in a collision with atomic electrons is not always the same since the distance of closest approach (impact parameter) is not predictable and varies considerably. The number of collisions suffered

by the projectile per unit length varies for individual protons. Therefore, the energy lost per unit distance traveled is not constant and so two protons with the same energy need not come to a stop at the same range or have the same pathlength. This variation is called *straggling* and it has a statistical nature. At low energies, where nuclear stopping dominates and where fluctuations in the effective charge of the proton are mostly prevalent, the fractional energy loss per collision becomes larger. Through nuclear stopping the proton undergos scattering resulting with the beam acquiring an energy spread after passing through a particular thickness of a target. This beam spread is known as *energy straggling*. Thus, a mono-energetic beam of protons do not have a unique range in the target material. The beam spread increases with increasing depth of penetration, resulting in *range* straggling. In short, range straggling is a consequence of energy straggling.

The Vavilov distribution [Vav57] is used to describe the energy straggling of charged particles. At low energies and large step sizes the Vavilov distribution approaches a Gaussian distribution [Sel64] while at high energies or small sizes the Vavilov distribution approaches a Landau distribution [Lan44].

2.2.4 Small-angle multiple scattering

During their passage in the matter the charged particles are deflected by the atomic nuclei. A single proton undergoes many such small angle deflections which may result in an increasing angular spread in the beam with increasing target thickness. This affects the beam such that it broadens towards the end of a thick target. The beam spread is caused by elastic nuclear collisions and the contribution from inelastic collisions are negligible [Sch01], [Wal92].

The Gaussian model based on the theory presented by Rossi [Ros42] is implemented in the treatment of small-angle Coulomb scattering. Although in the original theory both angle deflections and small spatial displacement were accounted for, however, in this model only the part of the theory that addresses the angular deflections is used for charged particles.

2.3 Nuclear interactions

The type of processes most prevalent when the charged particle traverses the target material depend on the type of interactions between the two ions. It is possible for the two ions to interact non-elastically through elastic Coulomb scattering. This happens when the distance between the interacting ions is large enough for them to feel each others field i.e. the particle does not come into close contact with the target nucleus. If the encounter is close enough, the projectile may produce an internal disturbance in the nucleus which may result in the excitation of the target nucleus. This process is refer to as *inelastic scattering.* At even closer encounters the incident projectile may penetrate the nucleus thereby causing a nuclear reaction. In this instance, the projectile can either collide with a single nucleon, ejecting it directly or it can get absorbed in the nucleus. The latter gives rise to the formation of the *compound nucleus* while the former results in *pre-equilibrium.*

There are three types of mechanisms that can take place in proton-induced nuclear reactions. *Direct* nuclear reactions takes place when the proton interacts with a few nucleons in the target, some of which are directly ejected and the majority of the nucleons are left undisturbed. In this

case there is a strong possibility that the proton will leave the nucleus again after losing a fraction of its kinetic energy to the nucleons. This reaction takes place very fast (within 10^{-22} seconds) i.e. without going through the compound nucleus stage. In the *compound-reaction* mechanism the proton is absorbed in the nucleus, resulting with the compound nucleus progressing towards a statistical equilibrium. This is due to the fact that the nucleons re-share and re-share the energy of the proton among themselves without any emission. The excited compound nucleus de-excites by emitting particles and gamma rays until it finally reaches the ground state. In contrast, compound-nucleus occurs at longer times (typically 10^{-16} seconds) compared to direct reactions. During this nuclear excitation, the energy of the proton is progressively shared amongst the target nucleons and at any stage particle emission can occur. A clear-cut classification into either direct or compound reactions is therefore often not possible since the so-called *pre-equilibrium* emission frequently occurs during the reaction.

In summary the interaction can be categorized into three stages, namely, first, second and final stage. In the first stage a particle incident on a nucleus interacts with individual nucleons via particle-particle cross sections as described by Bertini [Ber63] in a potential which describes the density of the nucleus as a function of radius. In order to describe this phase *Intranuclear cascade* (INC) and *Pre-equilibrium* models [Hod92] are used. In the second stage, the residual nucleus undergoes *evaporation* by releasing neutrons and light ions. Typical energies for evaporation are around 1 MeV. In the case of light ions (for $A < 13$ and $14 < A < 20$) a *Fermi-breakup* model replaces the evaporation model [Man24]. In the final stage the excited nucleus decays by gamma emission, when the excitation energy is below the threshold for

particle production.

In the intranuclear cascade (INC) model the particles propagate like free particles in the nuclear medium. During the interaction the nucleons are considered to be free gas, confined within a potential that describes a nuclear density as a function of radius. The Fermi motion of the nucleons is taken into account when modeling the interactions. The basic assumptions of the intranuclear cascade model revolve around

- the spatial point where the incident particle enters is selected uniformly over the projected area of the nucleus,
- total free particle-particle cross-sections and region-dependent nucleon densities are used to select the path length for the projectile particle,
- the exciton model is updated as the intranuclear cascade proceeds, and
- if Pauli's exclusion principle allows and the energy of the particle is greater than the cutoff energy, the second step is performed to transport the products.

The interaction probability per unit length is given by free space cross section, properly averaged over the Fermi motion of the target nucleons times the local nuclear density. Therefore, the particle motion is formulated in a classical way in that it can be subjected to an average nuclear potential, which is added to the kinetic energy of the particle when traversing through the nucleus. The effect of the nuclear mean field on the particle motion is either null (zero) or it produces curved trajectories in a semiclassical approach according to energy and momentum conservation. The curveture effects by the mean field are commonly refered to as "refraction" or "reflection" effects.

In principle, interactions occur like in free space in the Center of Mass System (CM) of the two colliding ions and because of the Fermi motion, the laboratory frame does not coincide with the frame where the target is at rest but a suitable Lorentz boost is applied to transform the secondary particles back into the laboratory frame. Interactions occur in a completely incoherent and uncorrelated way. No coherence or difractive effect is included and neither are cluster or multibody processes are included. Quantum effects are mainly limited to Pauli blocking. Secondary particles are treated in the exact same way as primary particles, with the only difference that they start their trajectory already inside the nucleus. The momentum of the target nucleus is described by the Wood-Saxon distribution where the potential, V(r), is in the form of several concentric spheres of different density as shown by the expression below

$$V(r) = -Vf(r) = -\frac{V}{1 + exp[\frac{r-R}{a}]}, \tag{2.3}$$

where R is about half density radius and a is the diffuseness parameter. In this case the nucleus is considered to be a cold Fermi gas. The INC model is less successful at low energies. The pre-equilibrium phase is the transition between the first reaction and final equilibrium hence at low energies it replaces INC model.

Two approaches are most commonly used to describe the pre-equilibrium phase, viz. quantum-mechanical multistep model and the exciton model [Hod92]. The initial number of "excitons" (a particle above the Fermi surface or a hole below the Fermi surface) is established. At each step the excited

nucleus may emit a neutron, proton, deuteron, triton, helium-3 or an alpha, or may even evolve toward an equilibrium number of excitons by increasing the exciton number by one particle-hole pair. The chain stops when either the exciton number or when the excitation energy is below any emission threshold.

2.4 Residual radioactivity

Most of the residual nuclei produced via nuclear reactions are unstable. In order to return to stability they subsequently decay either via alpha, beta, or gamma ray emission. Mainly neutron-deficient radionuclides which decay by means of positron emission accompanied with photon annihilation and also with other gamma rays, are produced this way. Electron capture and electron transition are other decay modes also common in neutron-deficient radionuclides. Hence, a production of a radionuclide usually result in a complex mixture of radiations, e.g. neutrons and gammas, which can be problematic especially to personnel and also to material and components of the target bombardment station. Therefore sufficient steps should be taken towards preventing the over-exposure of personnel and to limit the damage on the components.

2.5 Neutron interactions

Being one of the primary particle types emitted in a nuclear reaction, neutrons are produced in great numbers when a target material is bombarded with a proton beam. Unlike neutrons other light particles (protons, alphas, etc.) also produced are rapidly slowed down and stopped in or close to the

target. Since neutrons are uncharged they do not experience gradual slowing down when passing through matter. They interact only with nuclei hence they travel great distances in matter. The secondary particles resulting from neutron interactions are almost always heavy charged particles. These particles may be produced either as a result of neutron-induced reactions or by nuclei of the absorbing material itself, which has gained energy as a result of neutron collision. Consequently, they cause numerous secondary nuclear reactions not only in the material close to the target but also in the walls of the room in which the bombardment is performed. The relative probability of various types of neutron interaction change dramatically with neutron energy. Therefore, neutrons are categorized into two groups viz. "fast-neutrons" and "slow-neutrons".

Slow-neutron interactions include elastic scattering in which the neutron interacts with the absorbing material nuclei and a large set of neutron-induced nuclear reactions. Very little kinetic energy can be transfered to the nucleus in elastic scattering. This is mainly due to the small kinetic energy that the slow neutron possesses. Elastic collisions bring neutrons into thermal equilibrium with the absorbing material before a different type of interaction takes place, which is why slow-neutron energy range is mostly found among thermal neutrons. The real important slow-neutron interactions are from neutron-induced nuclear reactions because they can create secondary particles of sufficient energy to be detected directly. Since the incoming neutron has a low energy, the reactions must have a positive Q-value to be energetically possible. Hence the radioactive capture reaction, (n,γ), is often the most probable reaction and plays an important part in the attenuation of neutrons.

In the case of fast neutron interactions, the importance of scattering becomes greater because the neutrons can transfer a considerable amount of their kinetic energy in one collision, resulting in recoil nuclei produced as secondary particles. At each scattering point a neutron losses energy and is slowed down to lower energies. On the other hand, if the energy is high the neutron will undergo inelastic scattering with the nuclei. The recoil nucleus is hence elevated to an excited state during the collision, followed by subsequent deexcitation, with emission of a gamma ray. The neutron losses a great deal of its energy than it would in an equivalent elestic collision.

Thermal effects such as free-gas and molecular binding thermal treatments have to be taken into account when tracking neutrons. In this treatment the target nuclei are in motion as a result of non-zero temperature of the material. To best describe this effect an isotropic Maxwellian distribution of the target velocities is assumed. Accordingly, cross sections are the function of relative velocity between the neutron and the target. In a Maxwellian "sea" of targets mono-energetic neutrons *"see"* targets with a spectrum of relative velocities leading to Doppler broadening of the cross sections. Furthermore, the temperature has an impact on the kinematics of neutron collisions due to neutrons tendencies to thermalise to energies consistent with the material temperature.

In molecular binding thermal treatment the low energy-wavelength neutrons can interact with the lattice spacing of solids and the cross sections shows very uneven behavior in that each peak corresponds to a particular sets of crystal planes. It is found that in some directions coherent scattering

(interference of scattered waves) has a constructive contribution while showing an opposite effect (non-constructive contribution) in other directions. This brings about change in angular distribution (Bragg scattering). Molecular energy levels can play an important role in liquids and solids, especially, vibrational and rotational levels and also in cases where energy spacing is approximately 0.1 eV to a few eV below. Neutrons can loose or gain energy in discrete amounts thereby modifying the double-differential cross section i.e. thermal inelastic scattering. Thermal cross section, S(α,β), are designed to model neutron scattering as impacted by the binding of the scattering nucleus in solid, liquid or gas moderators.

2.6 Photon interactions

An excited nucleus de-exite by radiating photons with different energy ranges. In an electronic transitions in an atom only photons with low energies are emitted but high energy photons are from *nuclear bremsstrahlung*. The transport and the attenuation of the photons depend largely on the three major interactions namely: Incoherent scattering, photoeletric absorption and pair production as well as the other types of scattering. All these scattering processes lead to a transfer of photon energy to electron energy. The photon can disappear competely or it can be scattered at a significant angle at which it continuously interacts with other atoms.

Coherent scattering occurs when a photon interacts coherently with all the electrons of the target atom. It is also known as *Rayleigh scattering*, and it neither excites nor ionizes the atom. The photon retains its orignal energy after the scattering events. This scattering is often neglected because of minimal effect on photon energy and small changes in direction. The probability

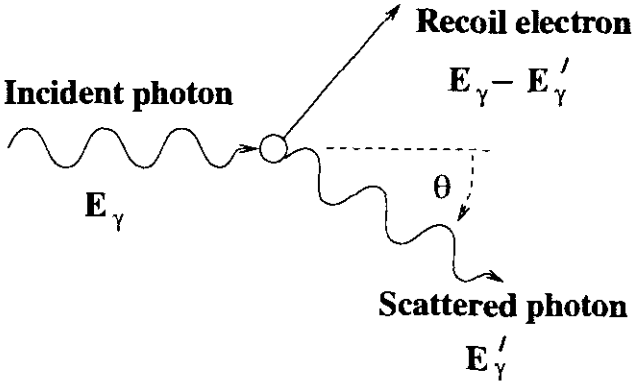

Figure 2.2: Schematic representation of scattering of a photon and an electron in the absorbing material.

of coherent scattering is significant only for low energy photons (i.e. few eV) interacting with low atomic number targets. The probability is most prominent when the interaction is with high atomic number targets.

The process of incoherent scattering take place when an incident photon interacts with an individual electron in a target material. The photon transfer a portion of its energy to the electron (assumed to be initially at rest) after the interaction. The electron is known as *recoil electron*. The photon subsequently continues to interact with other electrons until its energy is depleted at some angle with respect to its original direction. The electron then produces secondary ionization events. Thus, the angle of scattering depends on the energy transferred to the electron. Figure 2.2 shows Compton scattering which takes place between the incident photon and an electron in the

where

$$\bar{x} = \frac{1}{N}\sum_{i=1}^{N} x_i \tag{3.2}$$

and its relative error is given by

$$\sigma = \left[\frac{\sum_{i=1}^{N} x_i^2}{(\sum_{i=1}^{N} x_i)^2} - \frac{1}{N}\right]^{\frac{1}{2}} \tag{3.3}$$

If $x_1 = x_2 = ...$, then R=0 and if $x_1 \neq 0$, $x_2 = x_3 = ... = 0$, $R = 1$

The factors related to precision include the type of calcuations (forward versus adjoint), estimator type, variance reduction techniques and number of particles ran. Accuracy and precision are governed by the Central Limit Theorem which states that the distribution of the sum of independent, identically distributed random variables approaches a normal distribution as n approaches infinity [Man05].

The motivation for variance reduction is described by the relative error, R, as

$$R^2 = \frac{\sum_{i=1}^{n} x_i^2}{(\sum_{i=1}^{n} x_i)^2} - \frac{1}{n} = \frac{\sum_{i\neq 0}^{n} x_i^2}{(\sum_{i\neq 0}^{n} x_i)^2} - \frac{1}{qn} + \frac{1-q}{qn} \tag{3.4}$$

The first two terms of the equation represent the non-uniform (nonzero) scores while the last term represents the zero scores. The variance reduction technique strives to equalize the x_i scores as well as increase the fractions of

Chapter 3

MCNPX

3.1 Overview

MCNPX is a Monte Carlo radiation transport code developed at Los Alamos National Laboratory (US). This code was originally developed to transport neutrons and photons at energies up to 20 MeV hence the name MCNP. MCNPX was developed as a merge of the MCNP code and the LAHET code system (LCS) in 1994. In other words MCNPX extends MCNP to virtually 34 particles e.g. neutrons, protons, electrons, photons, 5 leptons, 11 baryons; 11 mesons and 4 light ions (deuteron, triton, helium-3 and alpha) at all energies. It is continuous in energy and direction. It treats arbitrary 3-dimensional geometry of materials in first or second-degree surfaces, tori, ten macrobodies and lattices. It uses continuous cross section data, with a range for neutrons, photons, electrons and protons that extend to energies up to 150 MeV and used physics models for energies extending above 150 MeV. This code can model inter-dependent source variables, seven estimator types and many modifiers.

absorbing material.

Photon interacts also through pair-production. This process occurs in the intense electric field near the protons in the nuclei of the absorbing material. The resulting effect is the creation of electron-positron pair. At the end of this process the incident photon disappears. Since the rest mass of the electron or positron is 0.511 MeV, therefore photons with energy greater than 1.02 MeV are required for pair production to take place. If the incident energy exceeds this value, the excess energy appears in a form of kinetic energy shared by the electron-positron pair. Therefore, the process consists of converting the incident photon into electron and positron kinetic energies. Since the electron and positron are charged particles they are therefore slowed down by the continuous Coulomb interactions with matter leading to the production of Bremsstrahlung photons, with energies far lower than that of the incident photon. When the positron has lost most of its energy, it recombines with a negatively charged electron. Both leptons disappear, and two annihilation photons are created, each with an energy equal to the rest mass of the electrons. The two produced annihilation photons move in opposite directions, at an angle approximately 180 degrees. The electron will interact with the surrounding nuclei.

In this study the models used in order to describe the processes taking place during the interaction of a proton and natural copper target are those implemented in MCNPX code. This code is discussed in detail in the following chapter.

MCNPX is supported on virtually all computer platforms e.g. Unix, Linux, Windows and parallel execution with PVM or MPI. It has a world-wide user base of more than three thousand, of which about two thousand are registered Beta testers [MCN05]. MCNPX has various applications, amongst which there is proton therapy, spacecraft, detectors, fuel cycle, radiation shielding, neutrino targets, etc. MCNPX can be accessed via the Radiation Safety Information Computational Centre (RSICC) at Oak Ridge National Laboratory [RSI05] and has limited access to the website [MCN05].

3.2 Monte Carlo technique

The idea behind Monte Carlo techniques is to model a physical system by statistically simulating individual physical events up to N times. With each complete simulations, information on system properties are gathered. Like in many other codes, the main concepts of Monte Carlo simulations are accuracy, precision, central limit theorem, tally mean (error) and tally variance.

Accuracy is defined as the measure of how close the true mean is to the physical quantity being estimated. This is sometimes refered to as the "systematic error". Monte Carlo codes cannot directly estimate this. The factors related to accuracy are: code accuracy (physics models, etc.) problem modeling (source, geometry, etc) and the user errors. On the other hand, precision is defined as the uncertainty in $\bar{X}_n$ caused by the statistical fluctuations in the sampled x's. Precision is sometimes called the "relative error" and is estimated by Monte Carlo codes. Precision is mathematically described as

$$R = \frac{\sigma_{\bar{x}}}{\bar{X}_n} = \left[\frac{1}{n}\left(\frac{\bar{x}^2}{\bar{X}_n^2} - 1\right)\right]^{\frac{1}{2}}, \tag{3.1}$$

nonzero scores.

The central moment of the history scores probability density function, f(x), relates to the mean, variance, confidence interval shift and the variance of variance. Therefore, a successful calculation should satisfy the following statistical checks:

- Mean should have a random behaviour.
- Relative error must be less than 5% for point detector simulations and less than 10% for other detector tallies. The half part should decrease monotonically by one over square root of N.
- Variance of variance should be less than 10% for all tallies and the last half should decrease monotonically by one over N.
- Figure of merit should have a constant value and show a random behaviour.
- History tally probability density function slope must be greater than 3.

The figure of merit (FOM) relates to the efficiency of the code, i.e. a measure of how quickly the desired precision is achieved. Monte Carlo codes estimate FOM from its relation to the relative error as well as on the time taken to complete the calculations. As such the FOM is given by

$$FOM = \frac{1}{R^2 T}. \tag{3.5}$$

where, $R^2 = \frac{1}{n}$ and T=n. The FOM should be constant with n and the larger it is the more efficient is the code. The factors affecting the FOM are the history-scoring efficiency, dispersions in the nonzero history scores and the computer time per history.

In summary the principle of Monte Carlo is the mechanisms for basic physical processes are known and individual processes are simulated by means of random numbers. Furthermore, the physics is used as a rule for the simulation. Subsequently, the random numbers are then uniformly distributed between zero and one. Due to the change in the system specifications the global properties of various physical system differs in terms of particle type, geometry energy, etc. However, the basic elementary steps by which the physics is modeled does not change.

3.3 Simulations in MCNPX

In order to perform MCNPX calculations the train of event start by visualizing the problem and also by understanding the type of modeling assumptions that are applicable for that specific problem. In short, two key questions need to be addressed are: can the actual geometry be reduced to a representative geometry and what quantity needs to be calculated for a particular system. A calculation is hence guided by the following basic steps:

- constructing a geometry
- defining material(s)
- defining a source
- histories / tallies

INPUT FILE
TITLE CARDS
CELL CARDS
[blank line delimiter]
SURFACE CARDS
[blank line delimiter]
DATA CARDS
[end line]

Table 3.1: A typical MCNPX input file showing different card types.

- running the calculation
- output

There are three kinds of default files associate with MCNPX, namely, input, output and the so called *runtpe*. The output is an *ascii* file while the "runtpe" is a *binary restart* file. The "runtpe" contains information relating to the number of particles, collisions and the time taken to complete the run. The input is a free-field format, non-case sensitive file which is composed of three basic card types given in Figure 3. The "cell cards" represent the so-called *hybrid data entry* in which the data is identified by a combination of both position and argument. The "surface cards" represent the *fixed data entry* where the data is identified by its positions relative to other data in the card while the "data cards" denote the *keyword data entry*. In the data card the data is identified by the arguments consisting of keywords and values.

The "data cards" are composed of information relevant to the particle type, source, material (nuclide), histories, estimators (tallies), variance reduction, etc.

3.3.1 Geometry

Plotting geometry entails constructing a simplified yet representative geometry of the problem. This is accomplished by labeling surfaces (as shown by the example in equation 3.6) and constructing cells (equation 3.7). The cells are composed by the combination of surfaces as well as material and its density (equation 3.8), and each cell must have a variance reduction. Hence they are the basic units of MCNPX!

$$\#\ \ SPH\ \ V_x\ V_y\ V_z\ \ R, \tag{3.6}$$

$$mt\#\ \ (+/-)density\ \ (+/-)surface\ \ imp:particle = 1, \tag{3.7}$$

$$mt\#\ \ ZZZAAA.id\ \ (+/-)fraction \tag{3.8}$$

The meaning of parameters in equation (3.6), (3.7) and (3.8) are as follows:

- # - surface/cell/material number
- SPH - spherical surface
- V - position (x,y,z) of the surface with respect to the cartesian plane
- R - radius in cm
- mt - material

- imp - variance reduction

Depending on the variable following (+/-), it denotes either the SI units or the cell sensor with respect to the surface number. For example, if (+/-) is followed by the density then it signifies the grams/cm^3 (-) or atom/barn-cm (+).

Different kinds of geometries can be plotted with MCNPX, e.g. spherical, cylindrical, box, rectangular, ellipsoid, etc. These are defined in the surface card (equation 3.6) where, depending on the structure of interest, a first, second or fourth order equation is used. The specification is by coefficients or points. Special boundaries types such as reflecting (mirror), white (isotropic) or periodic can be defined and most surface areas are calculated in MCPNX. Two geometries were modeled in this study.

Spherical geometry

The spherical geometry was modeled by considering the radiation shield as a concentric of spheres, with each layer represented by the sphere. The layers considered for the shield were iron (Fe), paraffin wax/boron carbide and lead (Pb). This is shown in Figure 3.1 where different layers depict the various layers of the shield. The total thickness of the shield was 64 cm, which consisted of 30 cm of Fe, 30 cm of paraffin wax/boron carbide and 4 cm of Pb.

For the spherical geometry the parameters that goes into the code are the: vertex, (x,y,z), and radius, R. In this study the spheres were considered as centered at origin, (0,0,0) and the radii (in cm) were 30, 30 and 4, respectively.

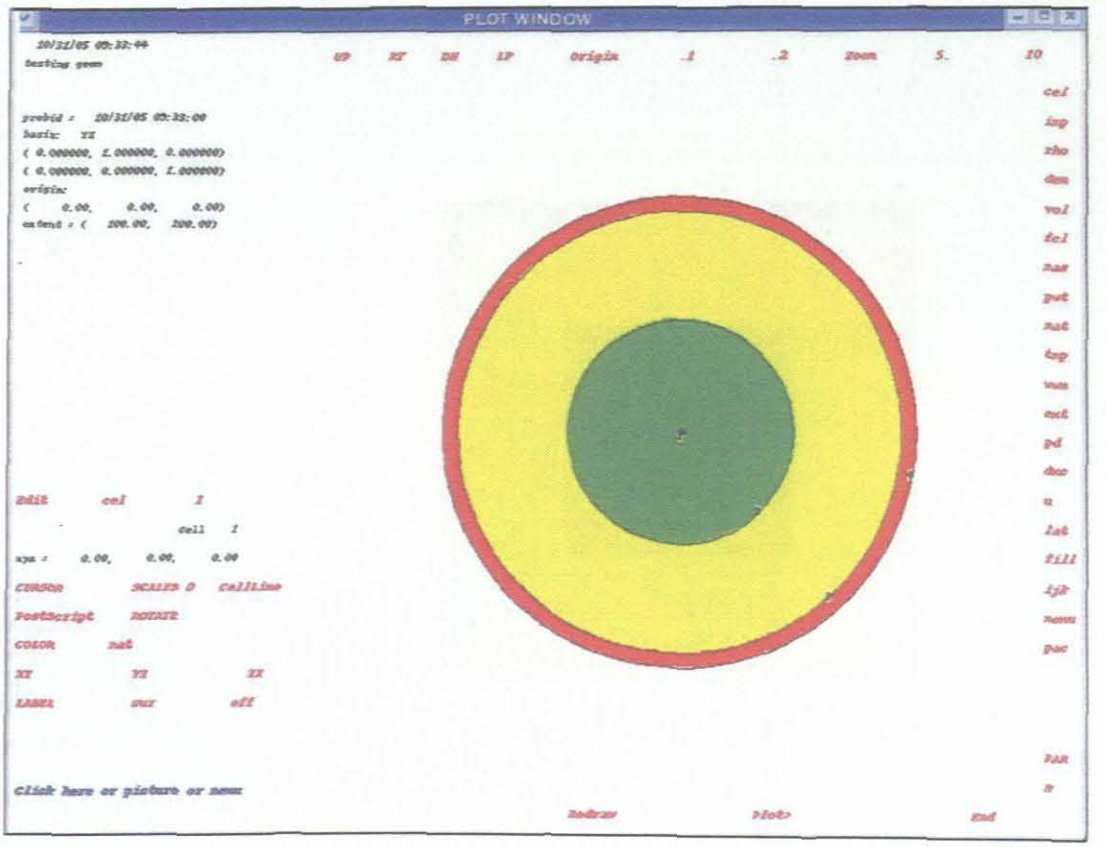

Figure 3.1: Illustration of the spherical geometry plotted by means of MCNPX. The green color represents Fe, yellow represents paraffin wax/boron carbide and red color represents Pb.

Cylindrical geometry

The general format for determining a cylindrical geometry is given by

$$RCC \;\; V_x \, V_y \, V_z \;\; H_x \, H_y \, H_z \;\; R. \tag{3.9}$$

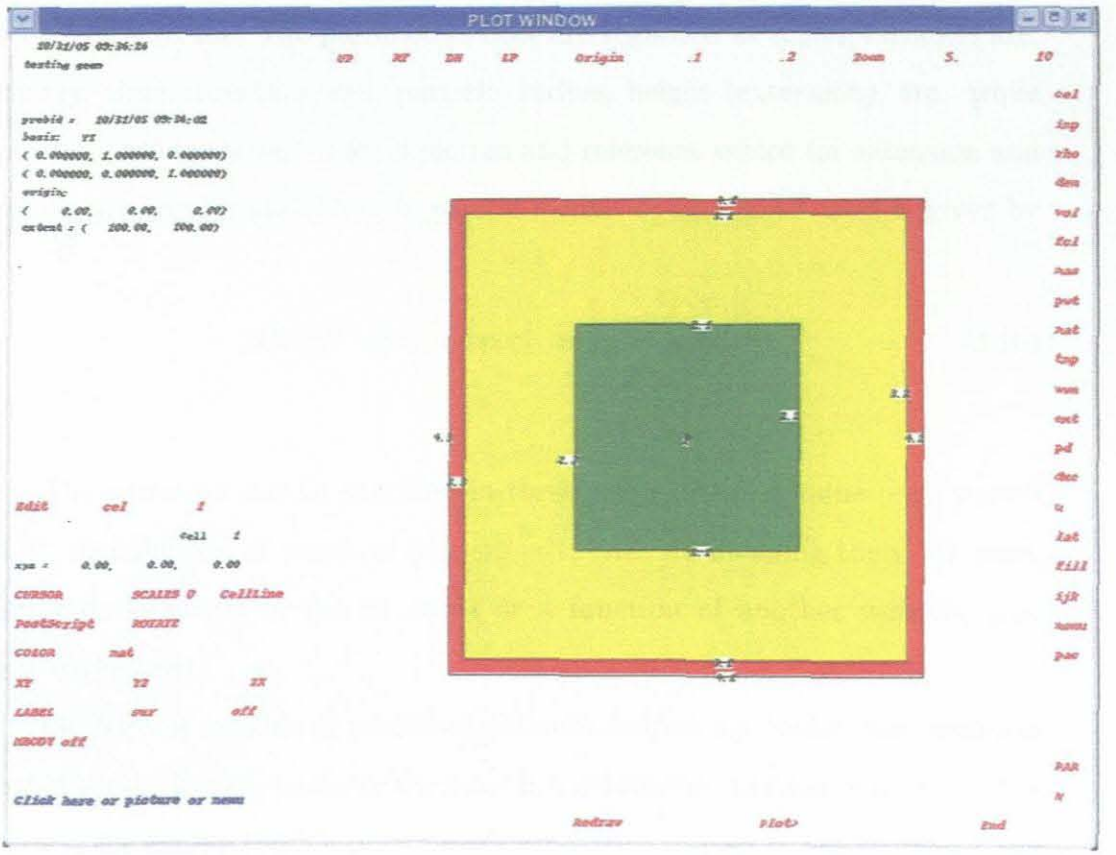

Figure 3.2: Cylindrical geometry by means of MCNPX. Green denotes Fe, yellow denotes wax/boron carbide and red denotes Pb.

In this work the parameters used to describe the cylindrical geometry, for example, of Fe were the vertex (0,-30,0), height (60cm) and radius (30.75cm). A similar trend was followed to describe all the other layers. The plot of the geometry is shown in Figure 3.2.

3.3.2 Source definition

In MCNPX the source type is defined by the kind of variables specified in the source definition card (SDEF). The variables can take a form of a scalar or

scalar or a vector. The parameters that are regarded as scalar variables are: energy, time, direction, cell, particle, radius, height (extension), etc. while position, reference vector for direction and reference vector for extension and radius are vectors variables. A general format of the *SDEF* card is given by

$$SDEF \quad var_1 = spec_1 \quad var_2 = spec_2 \quad ..., \tag{3.10}$$

The variables can be specified in three ways: explicit value (e.g. pos=0 0 0), distribution of numbers (e.g erg=d1, with d1 meaning there are more numbers following in the S1 card) or a function of another variable (e.g. erg=f(pos)=d1).

MCNPX is capable of modeling different sources e.g. point, line, uniform volume, etc. In each instance the most important information required by the code is the energy (MeV), position of source with respect to the geometry, the primary particle as well as the secondary particles (if any) to be transported. Two source types were modeled in this study and these are discussed below.

Isotropic source terms

An isotropic source is defined as a source that emits radiation equally in all direction. This source is completely independent of the angle of emission hence the information relevant to describe this source are the energy, the source position and the primary/secondary particle of interest. In this study source was the 66 MeV proton beam impinging on a copper target. The target was positioned at center (0,0,0) with respect to the geometry. The particles of interest were neutrons and photons.

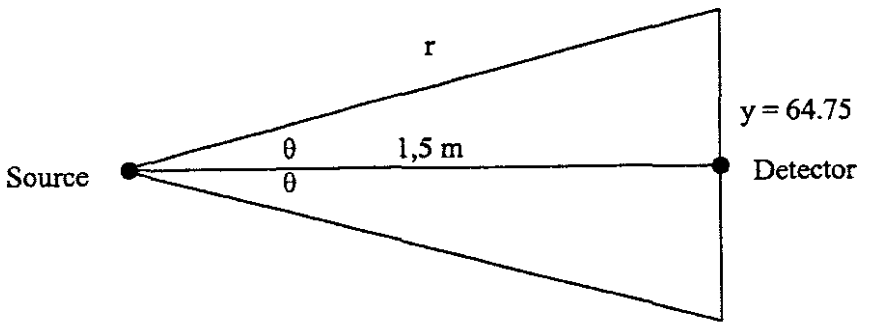

Figure 3.3: The schematic diagram depicts the angle and plane normal to the source used to describe the anisotropic source terms.

Anisotropic source terms

In anisotropic source the emitted radiation intensity is not rotationally symmetric about the normal to the source plane. The information relevant in defining this source, that is, in addition to energy, position and particle types, are direction (forward or backward), vector for position and the plane normal to the source as illustrated in the equation below and in Figure 3.3.

$$SDEF\ pos = 005\ erg = 66\ par = h\ dir = d1\ nrm = -1\ vec = 001. \quad (3.11)$$

The angle is described by *dir.* with *d1* meaning covering the angles -π and π in the forward direction (nrm=-1). *vec* is the position vector.

Neutron source strength

The total neutron source strength was estimated from the neutron yield, S, by making use of the yield obtained by Ryder [Ryd82] from protons up to

200 MeV on a thick Cu target. The value extrapolated from Ryder is

$$S = 6 \times 10^{11} \ \ neutrons.second^{-1}.\mu A^{-1}. \tag{3.12}$$

Therefore, a typical 66 MeV proton beam with current intensity of 100 μA, produces neutrons with a strength of 6 $\times 10^{13}$ neutrons/second.

Photon source strength

The total photon source strength was estimated from the photon yield by making use of the yield obtained by Zobel *et al.* [Zob68] where the source strengths were experimentally determined by folding the thick-target photon production cross section with the proton stopping power. The proton energies varied from 16 to 160 MeV. The source srength of

$$S = 1.07 \times 10^{12} \ \ photons.second^{-1}.\mu A^{-1} \tag{3.13}$$

was obtianed. Therefore the photon produced by the 66 MeV proton beam of currents of 100 μA had a strength of 1.07 $\times 10^{14}$ photons/second.

3.3.3 Material Card

As already mentioned the cell is composed of the combination of surfaces, material and its density as well as variance reduction. As such, each cell was filled with Fe, paraffin wax/boron carbide or Pb as shown below

$$m1 \;\; 26056 \;\; -1 \tag{3.14}$$

$$m2 \;\; 1001 \;\; -0.146 \;\; 6000 \;\; -0.838 \;\; 5010 \;\; -0.0156 \tag{3.15}$$

$$m3 \;\; 82208 \;\; -1 \tag{3.16}$$

where the contribution (by weight fraction) of each nuclide (iron, hydrogen, boron and lead) were represented by the 26056, 1001, 6000, 5010 and 82208, respectively.

3.3.4 Tallies / Estimators

The choice of a tally (method of calculating) depends on the physical quantity of interest i.e. on the desired result. Therefore, it is important to ensure that the selected tally has the correct quantity needed to obtain the desired result. Unlike in Deterministic codes where an equation is solved directly in order to calculate flux, heating, reaction rates, etc. Monte carlo codes statistically sample events (track length, surface crossing, collisions and next event) in order to calculate these observables. For example, to estimate flux (cell or surface) the code samples either a track length (cell) or a surface crossing (surface). Currently, MCNPX is capable of modeling 8 different tallies, many tally modifiers (energy, time, cosine, rection multipliers, dose, etc.) and special tallies (mesh tallies and gridconverters). In MCNPX the units of a tally are determined by the source, i.e. if the source is given in particles/second then the tally will be given in per second. However for the

purpose of this study we only concentrate on those tallies applicable in the calculation of dose rates and dose attenuation factors.

Calculation of particle flux

The flux is defined as the number of integrated particles per unit area. The tracklength, λ, is defined by the relation between the particle speed, v, and the change in time, dt. Therefore, the cell flux, ϕ, is defined as

$$\sum \frac{W}{V}.vdt = \sum \frac{W}{V}.\lambda \tag{3.17}$$

The variables W and V denote the particle weight and cell volume, respectively. The surface flux is given by

$$\sum \frac{W\delta}{\delta A|\mu|} = \sum \frac{W}{A|\mu|}, \tag{3.18}$$

where $\mu = \cos\theta = \frac{\delta}{\lambda}$. The flux is given in particle/cm^2.s^{-1}.

The flux was normalized by multiplying it with a relevant source strengths obtained as discussed in section 3.3.2.

Effective dose

MCNPX does not directly calculate the dose rate, however, it converts the estimated flux into dose rate using standard fluence to effective dose conversion coeffiecient of a specific radiation (emitted particles) given by the energy and its corresponding dose function, DE/DF. The absorbed dose, D, is the

amount of radiation delivered on a matter with mass per unit time. This quantity is defined by the equivalent dose, H, and the effective dose E_{eff}.

The equivalent dose is given by

$$H_M = \sum w_R \, . \, D_{T,R} \tag{3.19}$$

where $D_{T,R}$ is the average absorbed dose from radiation, R, in matter, M w_R) is the radiation weighting factor for radiations , R, and the sum is performed through all kinds of radiation that consitute the radiation field considered. The values for the photons weighting factor recommended by by ICPR is 1 while in the case of neutrons the values differ, depending on the energy of interest e.g. for thermal neutrons, 100keV - 2 MeV, the value is 20, for low energy neutrons, 2 - 20 MeV, the value is 10 and for fast neutrons, E greater than 20 MeV, the value is 5. The effective dose is the sum of the weighted equivalent doses in matter. It is given by

$$E_{eff} = \sum w_R \, . \, H_M \tag{3.20}$$

The conversion factors were obtained from the Radiation Protection Dosimetry data base [Fer97], [Cha01], [Boz01]. The dose rate was given in units of $(\mu Sv/h)(\text{particles/cm}^2.s^{-1})$.

Dose attenuation factors

The dose attenuation factor is given by the ratio of the dose rate with shielding and the dose rate without shielding:

$$Dose\ attenuation\ factor = \frac{dose\ with\ shield}{dose\ without\ shield} \tag{3.21}$$

The attenuation factors for various shield layers were determined as discussed below.

Determination of boron carbide content

This calculation was performed in order to ascertain the amoumt of boron carbide-to-wax mixing ratio that represents a good price-performing compromise. The concentration of boron carbide in the wax was systematically accomplished by increasing the amount of boron carbide (by weight percent) in wax from 0% to 10% in increments of 0.5% boron carbide into paraffin wax as shown in Table 3.2. The values for the neutron and photon dose rates obtained in this work are given in Appendix B.

Determination of the iron depth

This calculation was performed in order to determine ratio of wax to iron that would minimize the neutron absorbed dose attenuation factor for an iron/wax shield of 60 cm total thickness. This was accomplised by shifting the position of the iron/wax boundary through the shield. An inner and outer wax (conating boron carbide) were considered. The shield configuration was considered as a two-layered interface consisting of iron and wax (with an appropriate percentage of boron carbide). Basically, we started off with zero iron and 60 cm paraffin wax implying that the "detector" was on the outmost side of paraffin wax. Then, the iron layer was introduced in small discrete steps on the "source" side. The dose attenuation factors for neutrons and photons (only those that are produced by the neutron) were calculated at

Content of B_4C in Wax	Density	Fraction of elements		
		Hydrogen	Carbon	Boron
100% PW / 0% B_4C	0.9300	0.1486	0.8514	0
99.5% PW / 0.5% B_4C	0.9380	0.1479	0.8482	0.0039
99% PW / 1% B_4C	0.9459	0.1471	0.8451	0.0078
98.5% PW / 1.5% B_4C	0.9539	0.1464	0.8419	0.0117
98% PW / 2% B_4C	0.9618	0.1456	0.8387	0.0157
97.5% PW / 2.5% B_4C	0.9698	0.1449	0.8356	0.0196
97% PW / 3% B_4C	0.9777	0.1442	0.8324	0.0235
96% PW / 4% B_4C	0.9936	0.1427	0.8260	0.0313
95% PW / 5% B_4C	1.010	0.1412	0.8197	0.0391
94% PW / 6% B_4C	1.025	0.1397	0.8134	0.0470
93% PW / 7% B_4C	1.041	0.1382	0.8070	0.0548
92% PW / 8% B_4C	1.057	0.1367	0.8007	0.0626
91% PW / 9% B_4C	1.073	0.1352	0.7943	0.0704
90% PW / 10% B_4C	1.089	0.1338	0.7880	0.0783

Table 3.2: Calculations of boron carbide content needed to optimize the shield for neutrons and photons.

1.5 m from the centre of the target. The scenario below describes the way the shield was configured.

	Fe	Wax	
	$0cm$	$60cm$	
	$10cm$	$50cm$	
	$20cm$	$40cm$	
Source	$30cm$	$30cm$	**Detector**
	$40cm$	$20cm$	
	$50cm$	$10cm$	
	$60cm$	$0cm$	

The values of the neutron and photon dose rates obtained in this work are given in Appendix B.

Determination of the iron / paraffin wax interface

This calculation was performed in order to determine the optimal laocation of the 20 cm thick wax (containing born carbide) layer. The wax layer was moved through an iron/wax/iron shield with a total thickness of 60 cm. That is, the paraffin wax was shifted across "detector" side to "source" side.

	Fe	Paraffin Wax	Fe	
	$0cm$	$20cm$	$40cm$	
	$10cm$	$20cm$	$30cm$	
Source	$20cm$	$20cm$	$20cm$	**Detector**
	$30cm$	$20cm$	$10cm$	
	$40cm$	$20cm$	$0cm$	

The values of the neutron and photon dose rates are given in Appendix B while the dose attenuation factor results are discussed in the following chapter (Chapter 4).

Chapter 4

RESULTS AND DISCUSSION

4.1 Overview

As already mentioned in the introductory chapter the main aim of this study was to reproduce the data obtained by Steyn *et al.* [Ste92] where the multi-group discrete ordinate code was employed. In that study only isotropic source terms were modeled. Spherical and cylindrical geometries wer also modeled. This chapter gives a detailed account of the results obtained from calculations with MCNPX. The results presented in this chapter include the particle absorption cross sections, the particle flux and dose attenuation factors. The dose attenuation results are categorized under "isotropic" and "anisotropic" source terms. Where available, the results are compared with the published data of Steyn *et al.*

4.2 Particle absorption cross-sections

In MCNPX the permissible energy ranges for cross-section data tables of neutrons and photons are:

- Neutron phyiscs: 0 - 150 MeV
- Photons physics: 1 keV - 100 GeV (10^5 MeV)

Hence the total particle absorption cross section (in barns) is given as a function of the maximum data-table particle energy (in MeV). The plots of the absorption cross sections for neutrons and photons in iron, wax/boron carbide and lead are given in Figures 4.1 and 4.2.

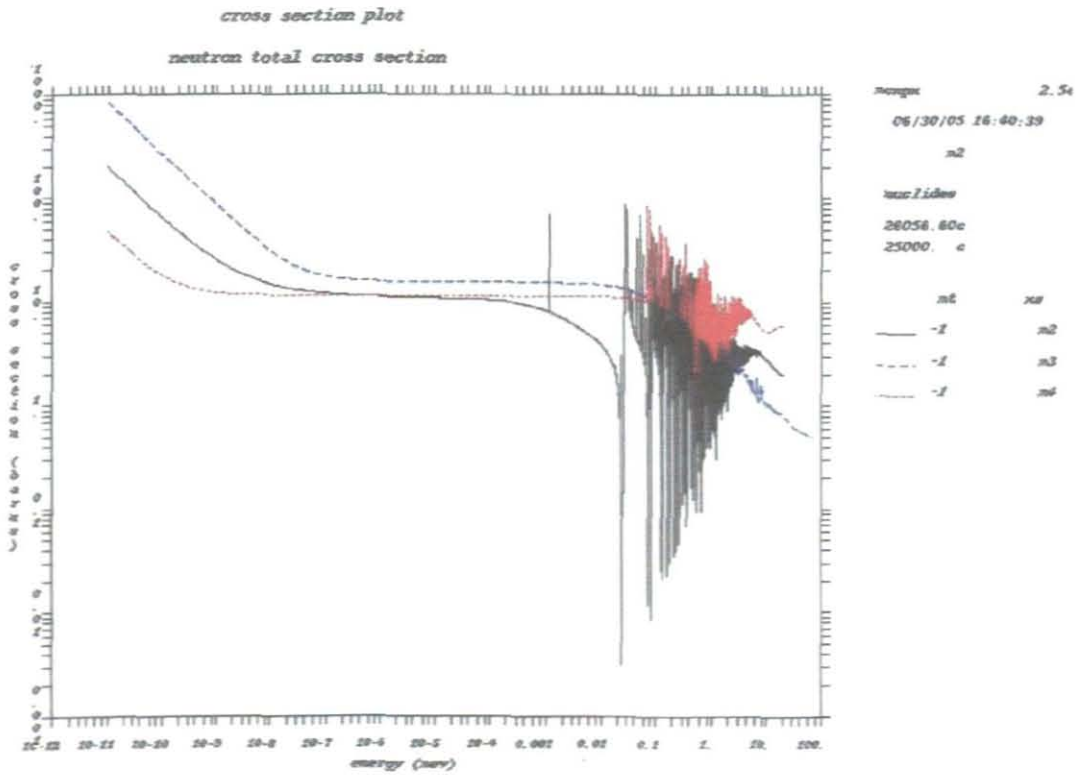

Figure 4.1: Graph showing neutrons as they propagate through iron (black), wax /3% boron carbide (blue) and lead (red).

Figure 4.1 shows the absorption cross section for neutrons in different layers of the shield. The cross section decrease with increasing particle energy

until a minimum is reached, after which it stays constant (plateau region) and then fluctuates sharply towards the end. Although this trend is evidenced in every layer of the shield but in comparison to the other layers Fe shows a much shorter plateau that has a shoulder-like decrease, which is immediately followed by sharp fluctuations. This makes the graph falls below that of lead. This behaviour is evidenced at data-table energies between 1 $\times 10^{-3}$ and 2 $\times 10^{-2}$.

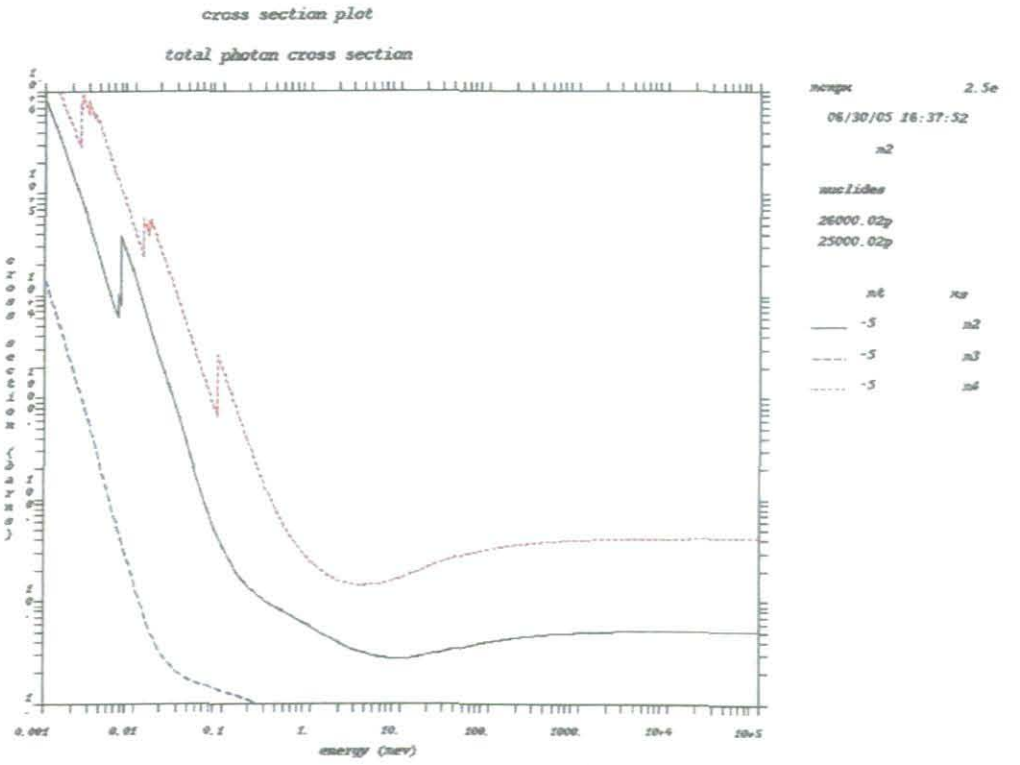

Figure 4.2: Graph showing photons as they propagate through iron (black), wax/3% boron carbide (blue) and lead (red).

Figure 4.2 shows a plot for the absorption cross-section of photons. The cross-section exhibits a rapid decrease with increasing data-table particle

energy until a minimum is a reached and then a gradual increase is evidenced. The shape of the graphs of Fe and Pb show a similar trend in that there are spuriuos and sharp hicups exhibited at occassional intervals. This is however not evidenced in wax. In Pb the cross section reaches a minimum at about 10 MeV, while in Fe the minimum is reached around 30 MeV. At low energies (1keV) the cross-section is very large (goes beyond 10^{6} barns) for Pb. This is about two magnitudes greater than in Fe.

4.3 Particle flux

The neutron and photon flux is plotted against the emission energy as shown in Figure 4.3 and Figure 4.4.

Figure 4.3 shows the flux for neutrons as they traverse through the shield. From the plot we can deduce that the neutrons are emitted with energies up to 60 MeV. From zero to 10 MeV the flux rapidly decrease to about 10×10^{-11} (n/cm^2/s). It then gradually decrease to almost 10×10^{-12} (n/cm^2/s) beyond 10 MeV.

In Figure 4.4 a plot of the photon flux for Fe, wax/boron carbide and Pb is shown. It is clear from the plot that photons are emitted with energies up 10 MeV. The flux fluctuates from 10×10^{-8} to about 6×10^{-11} (p/cm^2/s), with a drop to 10×10^{-11} at 8 MeV.

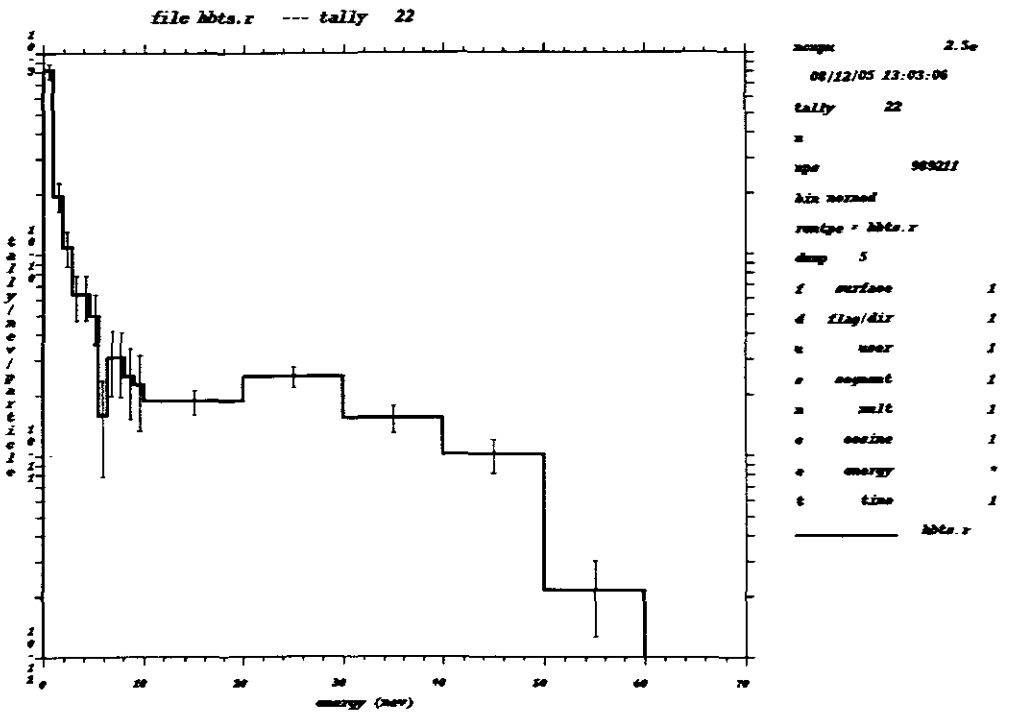

Figure 4.3: Calculated neutrons flux densities for the radiation shield consisting of leayers of iron, paraffin wax/3% boron carbide and lead.

4.4 Dose attenuation factors

The dose attenuation factors are presented in two categories, namely, isotropic and anisotropic source terms. In each case the data obtained for spherical geometry and also for cylindrical geometry is presented.

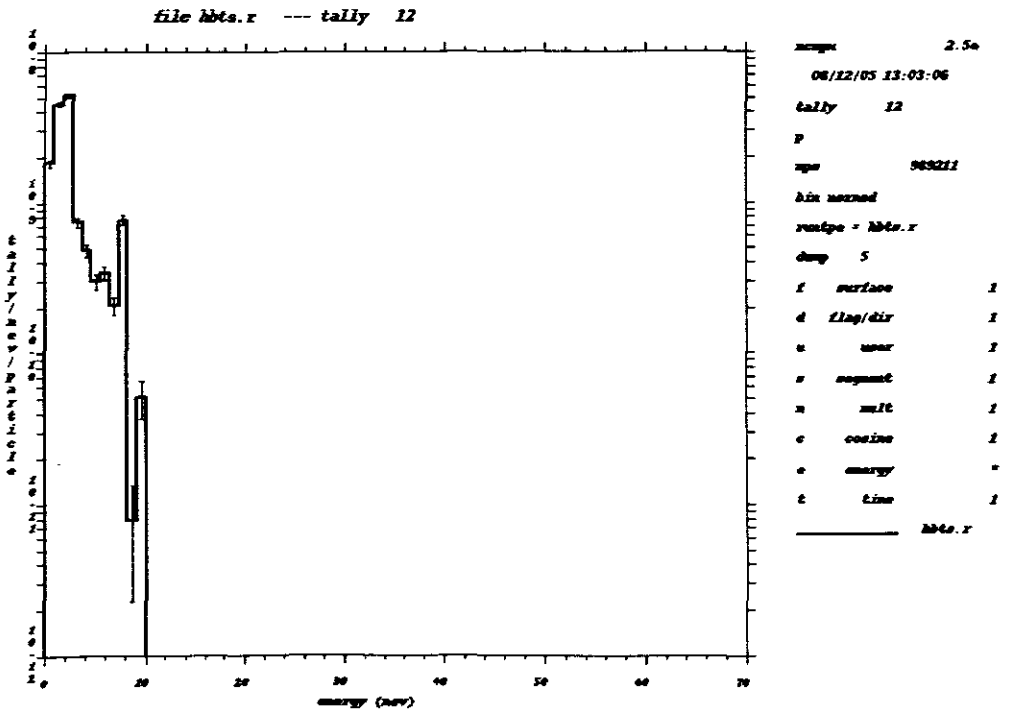

Figure 4.4: Calculated photon flux densities for the radiation shield consisting iron, paraffin wax/3% boron carbide and lead..

4.4.1 Isotropic source

Spherical geometry

In Figure 4.5, a plot of neutron and total dose attenuation factors as a function of boron carbide content is shown. The total dose attenuation factor decreases rapidly from a value of 0.018 to 0.0063 between 0% and 0.5% boron carbide content after which it shows a slight decrease until at about 3% where it remains almost constant at a value of 0.005. While Figure 4.6 shows the neutrons and total dose attenuation factors as a function of iron/wax depth (thickness). In this case the dose attenuation factor, specifically that of neu-

trons shows a gradual decrease until about 42 - 44 cm where a minimum value of 0.004 is reached. After that thickness it increases gradually to 0.005 and increases sharply to almost 0.2 at the thickness of 60 cm iron/wax. The figure that depicts the calculation performed in order to determine the best position for iron (inner or outer) with respect to paraffin wax is given by Figure 4.7. Similarly, the neutron as well as the total dose attenuation factors are plotted as a function of iron/wax depth. In this case both dose dose attenuation factors show a linear decrease with the thickness of iron/wax, with an exception after 30 cm where the total dose increases from a value of 0.009 to 0.02.

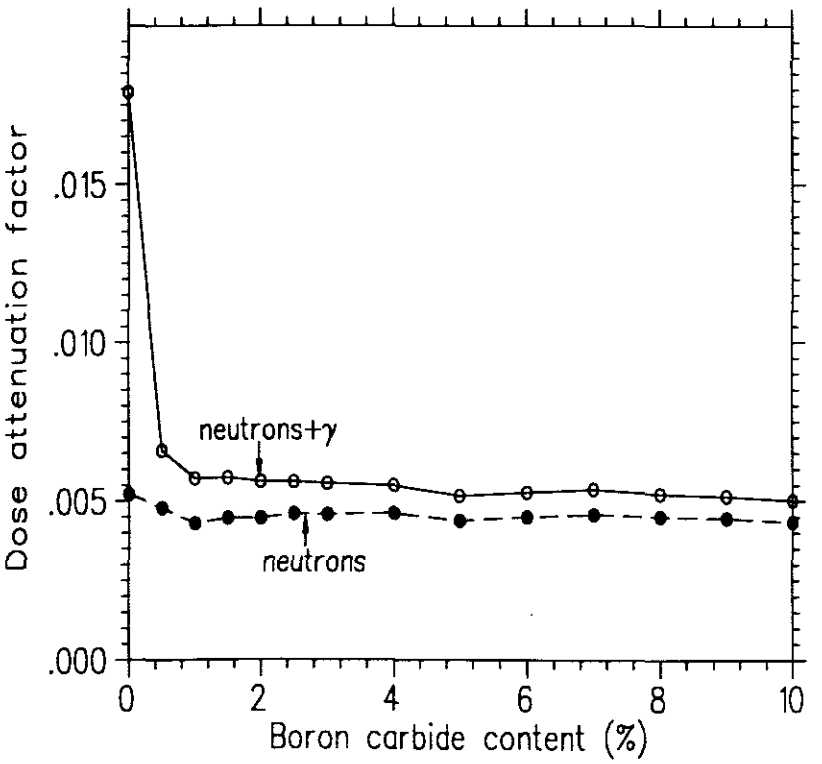

Figure 4.5: Calculated neutron and total dose attenuation factors at 1.5 m from centre of source for a 64 cm thick iron(60 cm)/wax(20 cm)/lead(4 cm) spherical geometry, as a function of boron carbide mixing ratio.

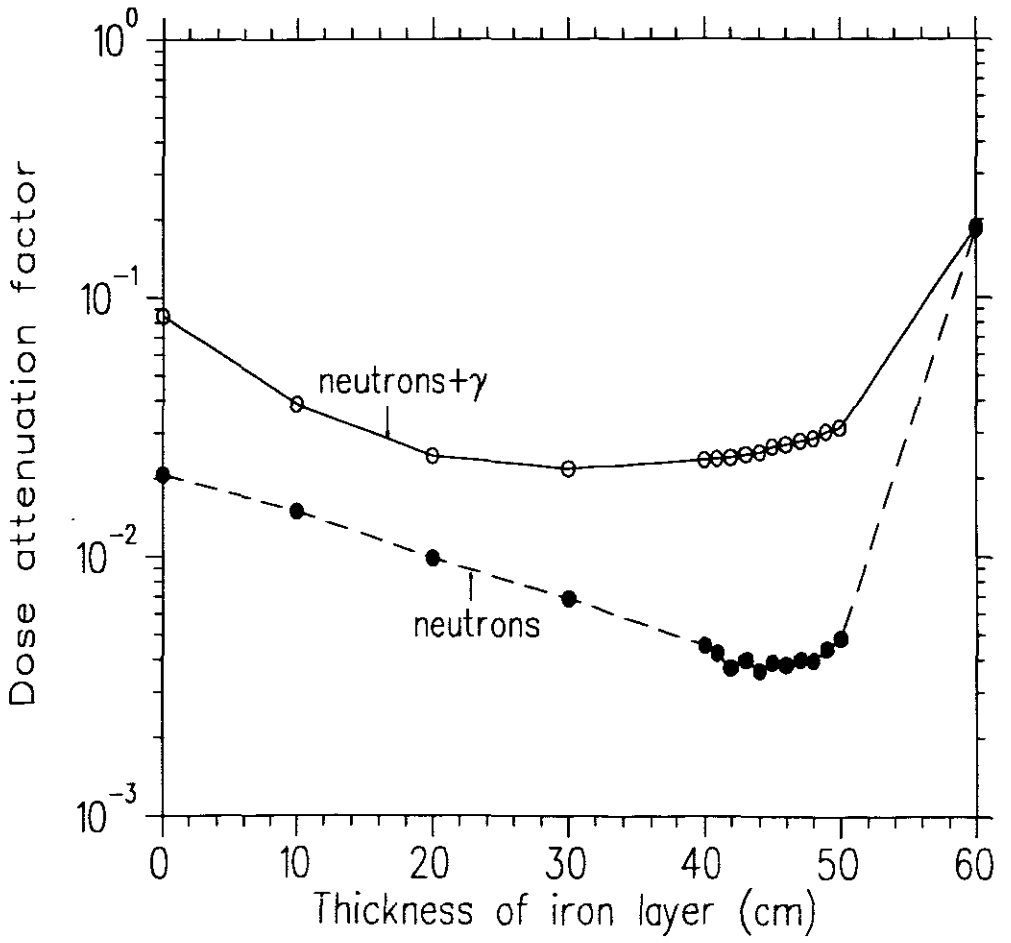

Figure 4.6: Calculated neutron and total dose attenuation factors at 1.5 m from centre of source for a 60 cm thick iron/wax spherical shield, as a function of Fe layer thickness. The wax contains 3% boron carbide.

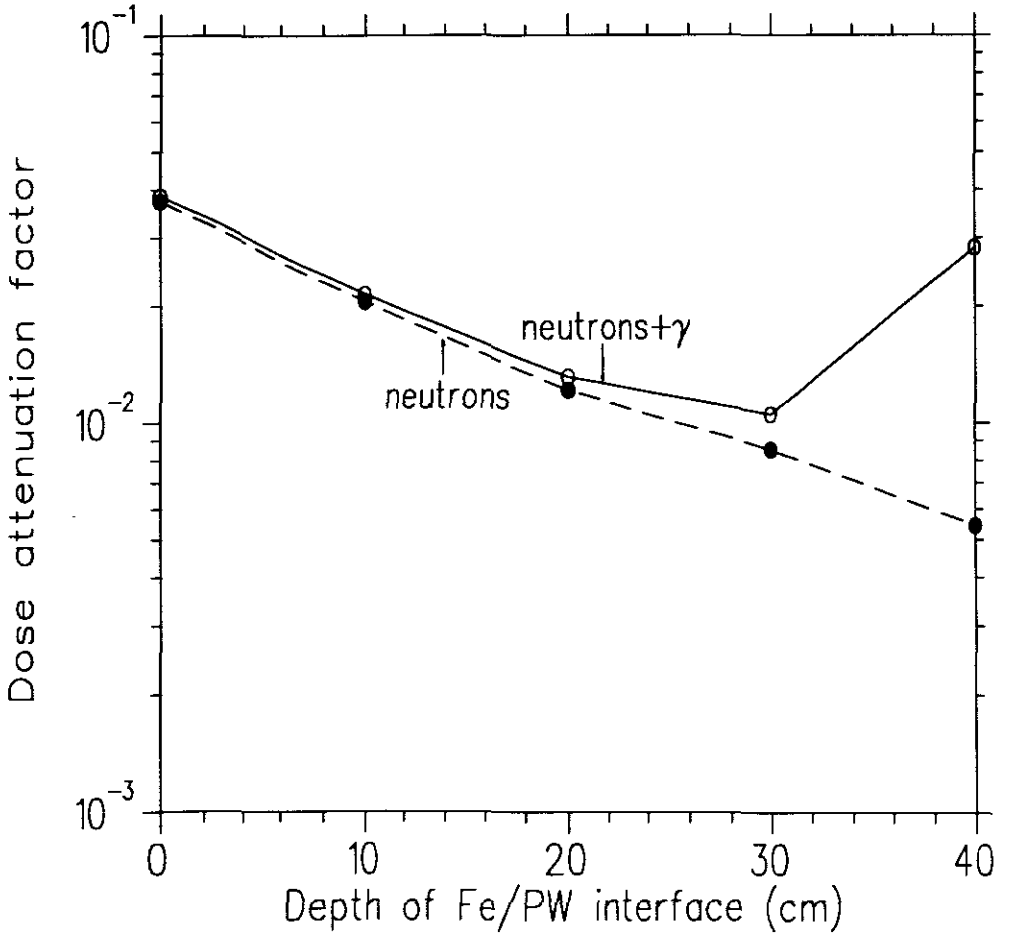

Figure 4.7: Calculated neutron and total dose attenuation factors at 1.5 m from center of target for a 60 cm thick Fe/wax/Fe spherical shield, as a function of Fe/wax depth. The thickness of wax is fixed at 20 cm.

Cylindrical geometry

The neutron and total dose attenuation factors were also calculated here. These are presented in Figure 4.8, 4.9 and 4.10, respectively. The trend witnessed for spherical geometry is also shown by the dose attenuation factor in this case however the attenuation factor has decreased slighly in this case. Overall, the value of the dose attenuation factor has decreased by a factor of about 0.23 in comparison to the values obtain for a spherical geometry!

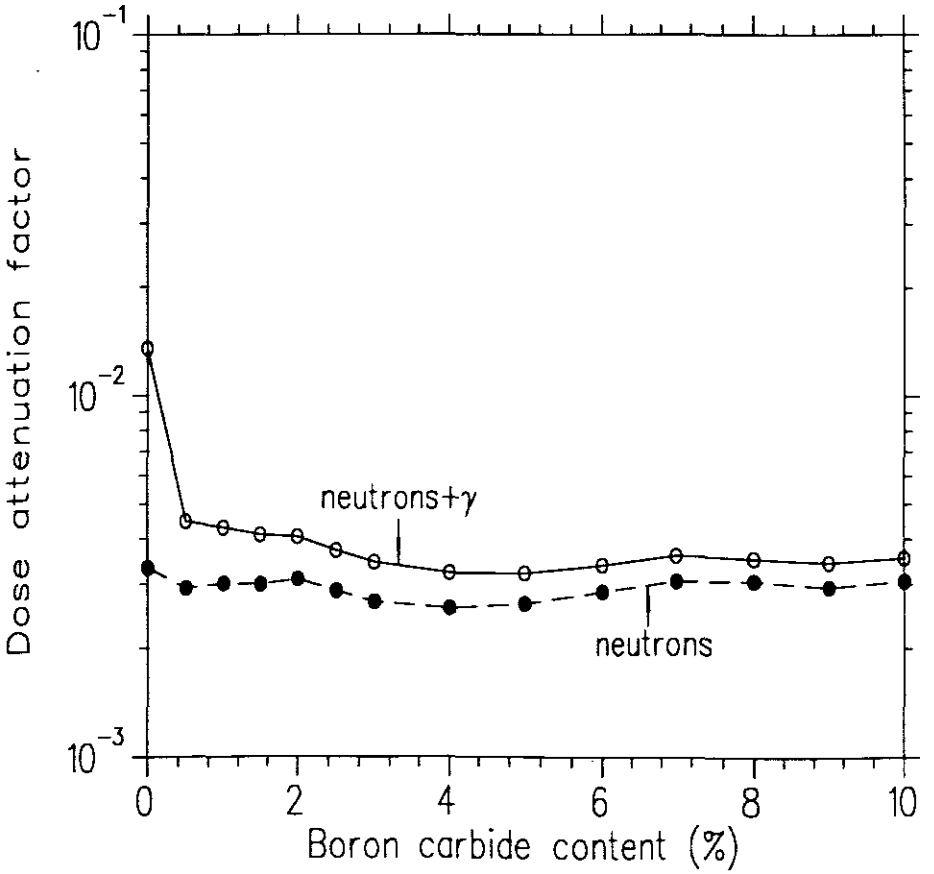

Figure 4.8: Calculated neutron and total dose attenuation factors at 1.5 m from centre of source for a 64 cm thick iron(60 cm)/wax(20 cm)/lead(4 cm) cylindrical geometry, as a function of boron carbide mixing ratio (by weight).

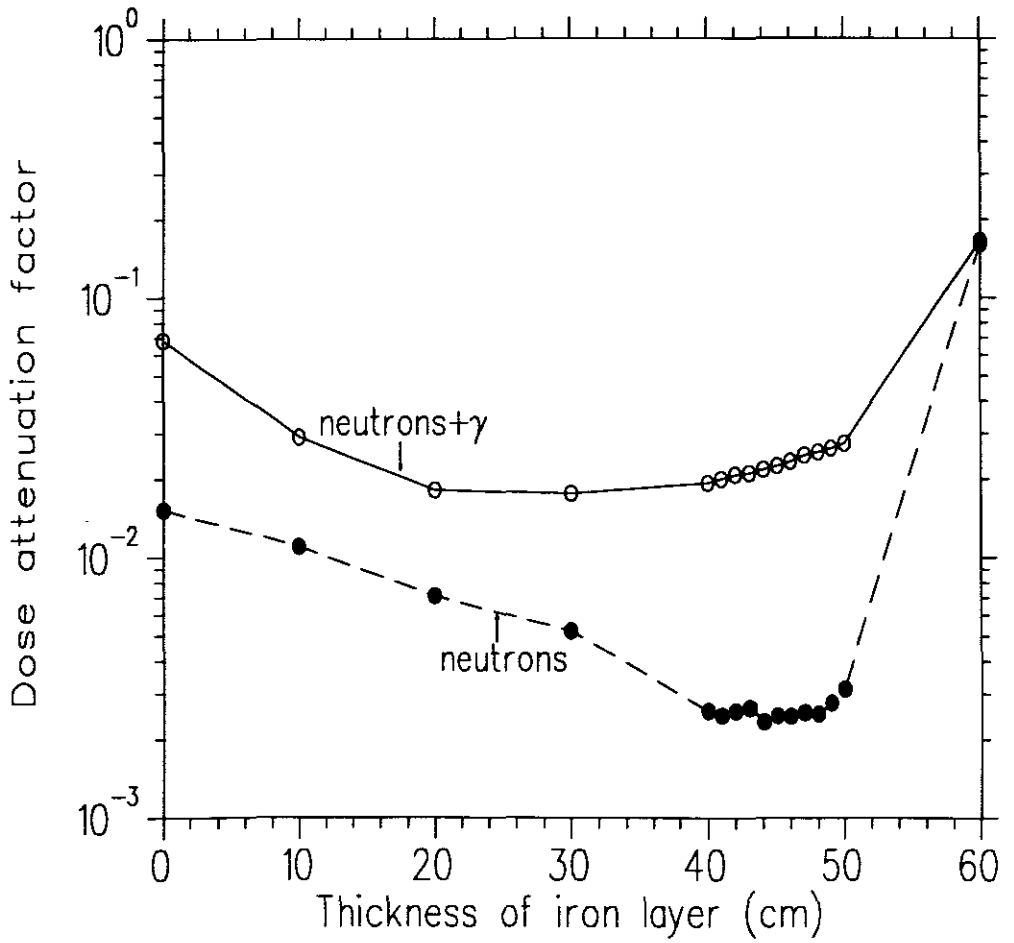

Figure 4.9: Calculated neutron and total dose attenuation factors at 1.5 m from centre of source for a 60 cm thick iron/wax cylindrical shield, as a function of Fe layer thickness. The wax contains 3% boron carbide.

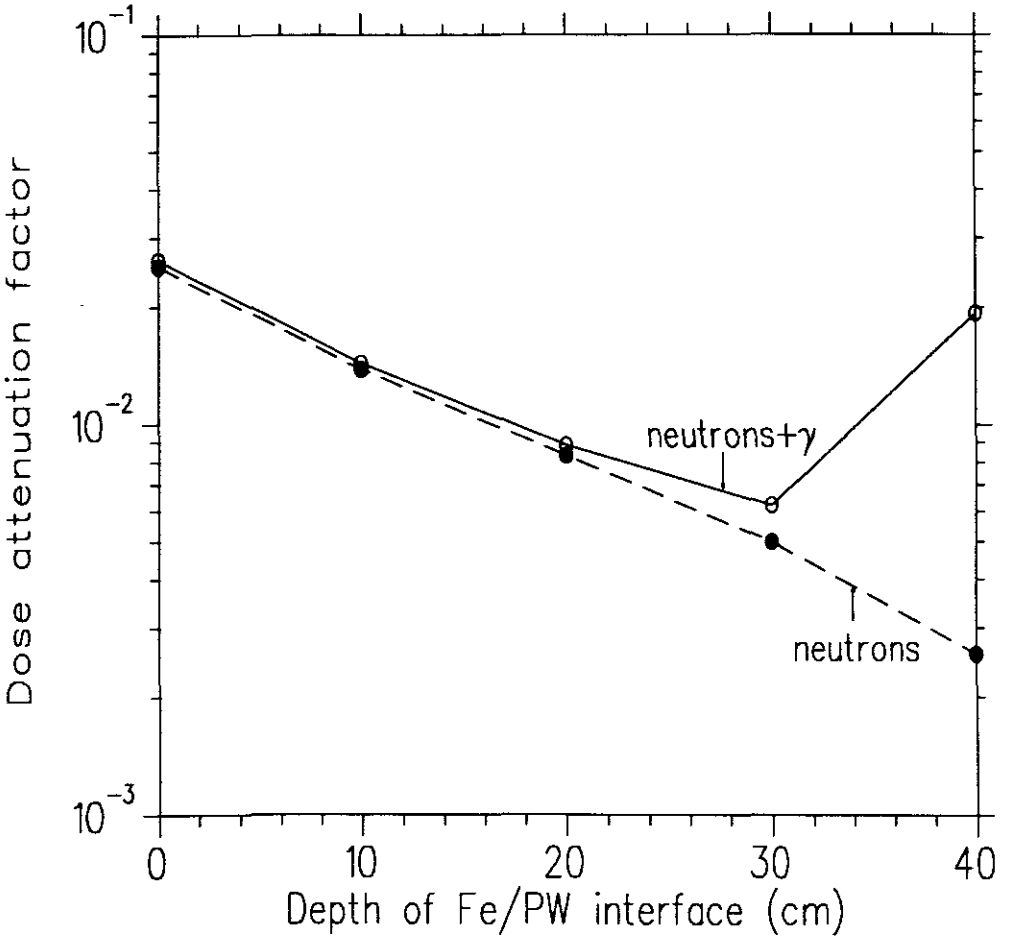

Figure 4.10: Calculated neutron and total dose attenuation factors at 1.5 m from center of target for a 60 cm thick Fe/wax/Fe cylindrical shield, as a function of Fe/wax depth. The thickness of wax is fixed at 20 cm.

4.4.2 Anisotropic source terms

The anisotropic source was modeled as discussed in section 3.3.2 (Chapter 3). Here we present only the spherical geometry. The results are shown in Figures 4.11 to 4.13, where the respective graphs present determinations of boron carbide mixing ratio, thickness of inner iron layer and the position of the inner iron/wax. Again, the shape (trend) of the dose is the same as those shown in the above sections. There is an overall improvement of about 17% to the dose attenuation factors. With anisotropic source terms Figure 4.12 shows that the value of the optimal configuration is an iron layer of about 46 cm, implying that the thickness of wax should be at least 14 cm!

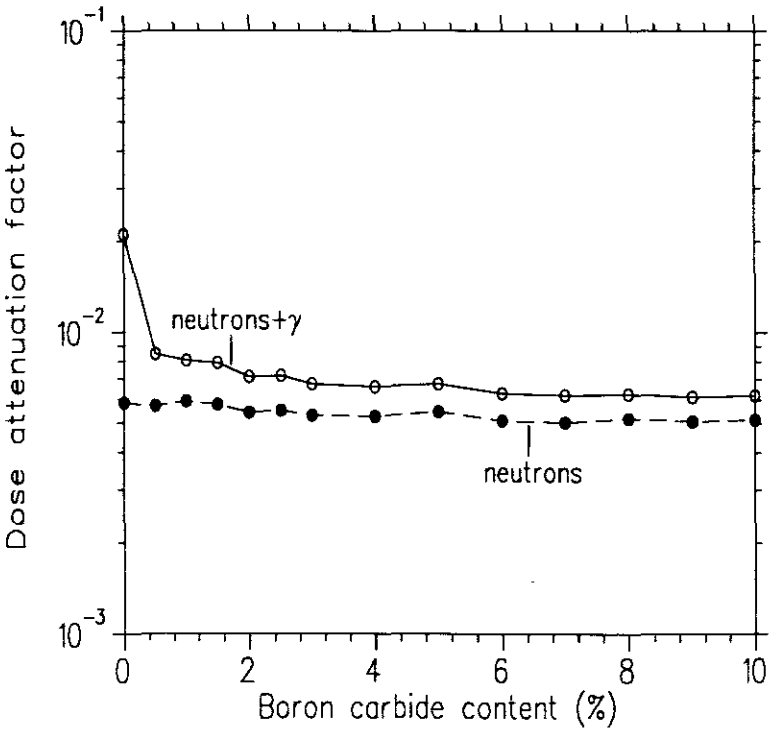

Figure 4.11: Calculated neutron and total dose attenuation factors at 1.5 m from centre of an anisotropic source for a 64 cm thick iron/wax/lead sphericical geometry, as a function of boron carbide mixing ratio.

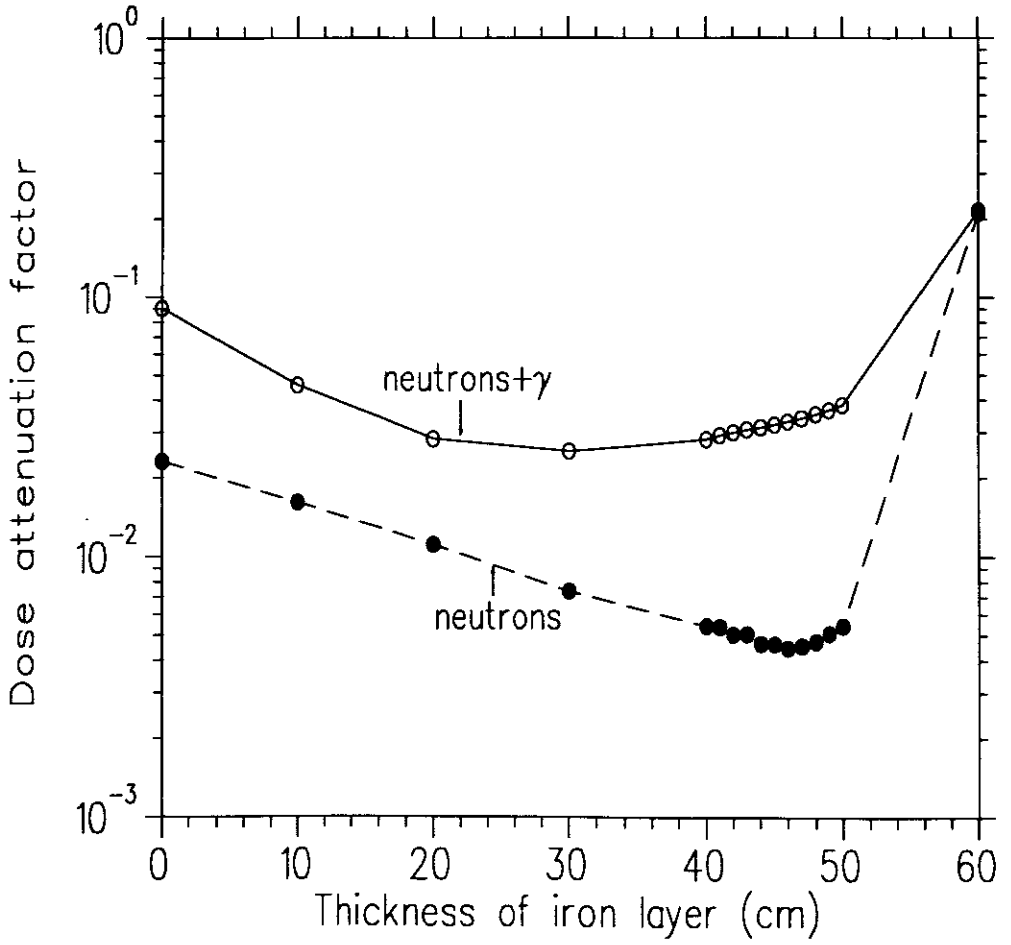

Figure 4.12: Calculated neutron and total dose attenuation factors at 1.5 m from centre of an anisotropic source for a 60 cm thick iron/wax spherical shield, as a function of Fe layer thickness. The wax contains 3% boron carbide.

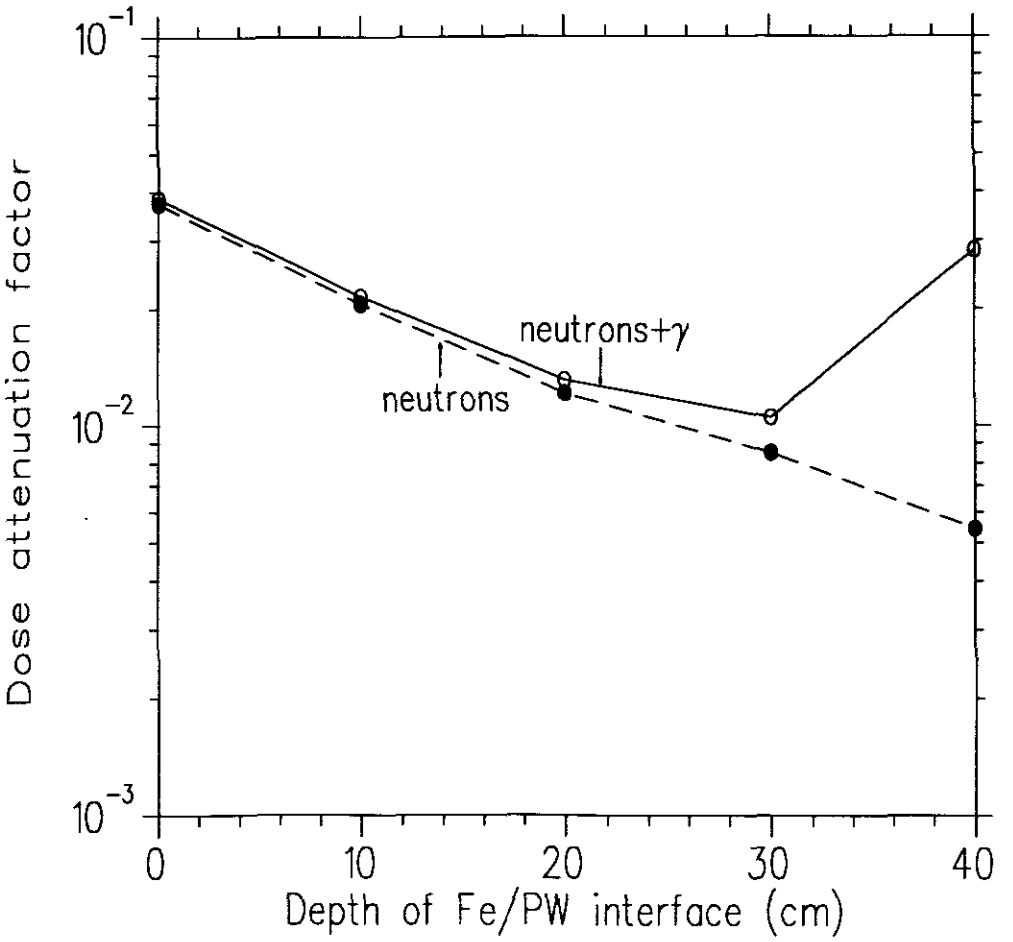

Figure 4.13: Calculated neutron and total dose attenuation factors at 1.5 m from center of an anisotropic source for a 60 cm thick Fe/wax/Fe spherical shield, as a function of Fe/wax depth.

4.5 Previous data

The results obtained from this present study were compared with those previously obtained by Steyn *et a.* [Ste92] where the multigroup discrete ordinate code was employed. Due to lack of availability of numerical values the data of Steyn *et al.* is presented in a seperate figure (Figure 4.14). These data were taken exactly as they are presented in the publication. In the figure the dose attenuation factors given as a function of (a) thickness of iron (b) thickness of Fe/wax interface, and (c) boron carbide content, respectively.

If we compare Figure 4.5 with Figure 4.14(c), there is a clear difference in the way the attenuation factor drops between 0 and 1% boron carbide mixing ratio. (Note that Figure 4.14(c) is in linear scale!) The previous data shows a curvy drop while the present data shows a linear drop. However in both cases the dose drops gradually until its constant. The good price-performance ratio was attained at 2.5% while a value of 3% was determined in this study. Furthermore, Figure 4.14(c) shows a huge difference of approximately 80% between the neutron and the total dose attenuation factors while the difference shown by MCNPX is about 29%.

Regarding the optimal configuration presented by Figures 4.6 and Figure 4.14(a), the value of about 0.0012 is achieved at 40 cm iron layer while in this work the value of 0.004 is reached at 40 cm iron layer. There are similarities in the shapes of the dose functions, though. Figures 4.7 and 4.14(b) show quite a difference in the way the dose drops off and picks up again. For instance, the change in the dose rate in Figure 1.14(b) is a smooth hyperbolic curve while Figure 4.7 shows a sharper change in dose. In both cases the neutron dose show a linear decrease however, the contribution of these neutrons to the total dose rate far less (5 time less for Figure 4.7 and 7 times less for Figure 4.14(b)) when the depth of the inner iron/wax interface is 30 cm.

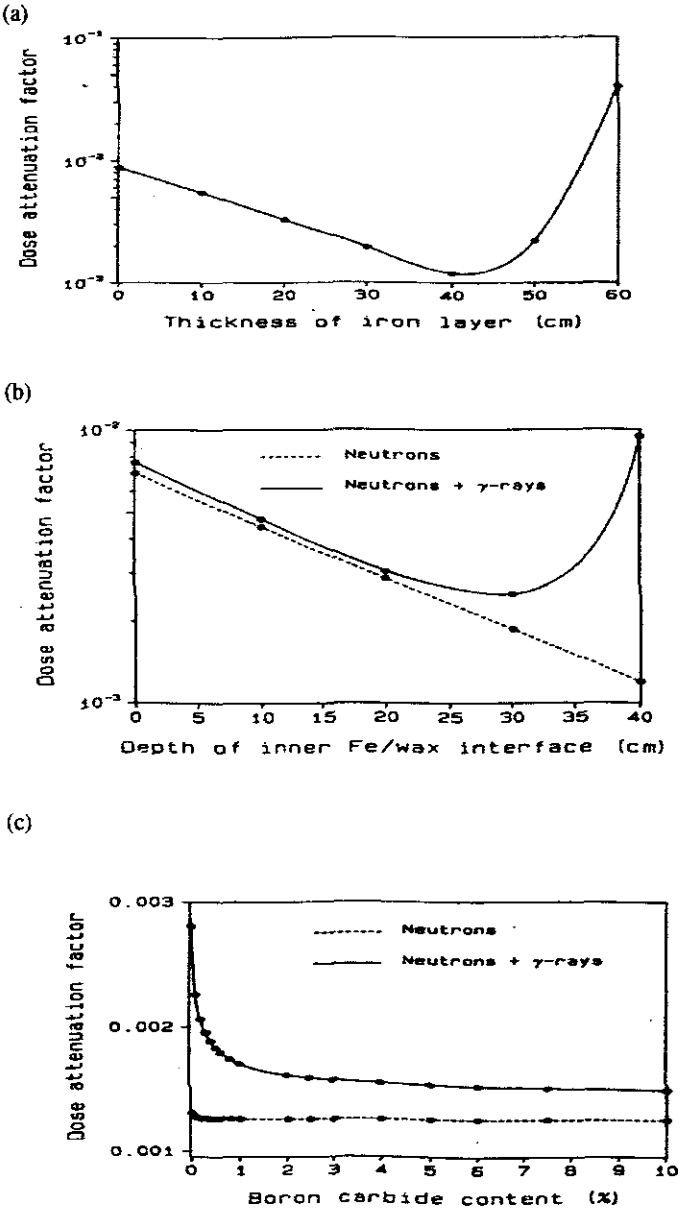

Figure 4.14: Neutrons and total dose attenuation factors as a function of the respective (a) thickness of Fe, (b) depth of Fe/wax and (c) boron carbide content, as obtained by Steyn *et al.* [Ste92].

Chapter 5

CONCLUSION

This thesis describes MCNPX simulations for the local radiation shield of the radionuclide production target bombardment station at iThemba LABS. The study had two main objectives. In the first case we had to reproduce the data obtained previously by means of the multigroup discrete ordinate code [Ste92] while the second motive was to model anisotropic source terms which could not be modeled previously. The reason for modeling anisotropic source was to check the accuracy of the results. In order to accomplish the first objective conditions such as isotropic source terms, cylindrical and spherical geometry terms were maintained. The results obtained in the first case were compared with those published by Steyn *et al.* [Ste92] and ultimately, isotropic source terms were compared with anisotropic source terms.

As a point of departure, the shield designed was optimized by varying thicknesses of layers or varying positions of material boundaries one by one while others were kept constant. In this way an optimal value for these specifications could be selected simply by observing the response of the transmitted absorbed dose rate. This process was repeated until an ideal optimal shield

design configaration was achieved within the initial boundary conditions. In principle, designing a radiation shield requires various homogeneous materials that are more practical for a given situation. This is evidently shown in this study by the different and complexity of the chosen materials. Because of the proximities within the target bombardment station at iThemba LABS the distance of 1.5 m from the centre of the source is a practical distance at which maintanance is perfomed.

The multigroup discrete ordinate code underestimated the dose attenuation factor at which the optimal configuration is acheived by a factor between 4 to 7 times less than that predicted by MCNPX. Secondly, according to MCNPX the optimal configuration is an iron layer of about 46 cm thickness together with a wax layer of about 14 cm. The wax should contain the boron carbide mixing ratio of about 3%. However, there is an agreement between the two codes in that they both predict that it is more practical to employ a shield consisting of an inner iron/wax layer (neutrons shield), and an outer thin lead layer (gamma ray shield) where the iron is on the "source side" and the lead is on the "detector side". The discrepancies between the two set of data can be attributed to the the fact that in order to achieve these calculations with the multigroup discrete ordinate code, two codes had to be employed in order to model spherical and cylindrical geometries, although same library was used in both cases. To model the spherical geometry ANISN (RSIC CCC-254, [Eng73]) was employed and DOT 3.5 (RSIC CCC-267, [Rho73]) for cylindrical geometry. Furthermore, isotropic source terms are useful only as rough estimates while an accurate indication of the dose can be estimated with anisotropic source terms because the emitted radiations are dependent on the angle of their emission, implying that the dose

rate depends on the angle of emission! In MCNPX one can model various geometries (spherical, cylindrical, cone, box, etc.) and many different source types (point, line, volumetric, etc)!

The absorption cross sections of neutrons and photons in Fe, wax, boron carbide and lead shown in the results confirms the effectiveness of a shield configured by a combination of material which compliment each other in terms of their ability to absorb or stop certain particles. For example, the combination of the high-atomic number material (iron) and a material with a great proportion of hydrogen and boron (paraffin wax/boron carbide) also illustrates the advantages of using these materials in order to stop neutrons. The inner iron layer effectively reduces fast neutrons to intermediate energies via nonelastic nuclear interactions while in the second layer neutron of about 4 MeV are moderated to thermal energies by elastic scattering due to the hydrogen in the wax. These thermal (slow) neutrons are then absorbed by boron-10 (^{10}B). This reduces the magnitude of the thermal neutron flux leaking from the wax and also decreases the 2.23 MeV photon dose rate outside the shield. These photons are emitted during the neutron capture by ^{10}B which has a high propensity to capture slow neutrons than does ^{11}B. The reaction, ^{10}B(n,α)^{7}Li, was first characterised by Taylor and Fermi and others in 1934 [Tay58], [Fer35]. The outer lead layer serves to attenuate both the 2.23 MeV photons as well as those residual photons from highly-activated targets and/or beamline components after irradiations. In this way the dose level is to maintainance level.

Overall, we can deduce that MCNPX has satisfactorily reproduced the previous data. The results from this study serves as benchmark for the design

of the newly installed Vertical Beam Target Station at iThemba LABS. Furthermore, results assures that MCNPX can be further applied in radionuclide production studies such as modeling complex targetry systems beam profile, heat transfer calculations as well. Also, MCNPX would would be very useful for the study of the newly installed Flourine-18-FDG (^{18}F-FDG) targetry system as well.

Chapter 6

APPENDIX A - Typical MCNPX output file

The output file contains input information as well as tables. There are about 33 tables in total. Some of these tables are default and some can be turned-off. The most important tables are given with their corresponding table number.

- Material composit4ion - 40
- Cell volumes and masses - 50
- Cross section data summary - 100
- Transport particles and energy limits - 101
- Source variables for the first 50 histories - 110
- Problem summary table
- Activity by cell - 126
- Tally data and/or Keff summary table

- Tally statistical analysis summary page - 160
- Printed plot of probability density function - 161
- Tally fluactuation chart

An example of a typical MCNPX output is given below.

```
mcnpx     version 2.5e  ld=Mon Feb 23 08:00:00 MST 2004              01/29/06 21:46:24
 ...............................................................................  prohid =   01/29/06 21:46:24
 i=hbts o=hhts.o r=hbts.r

 ******************************************************
 *                                                    *
 *            Copyright Notice for MCNPX              *
 *                                                    *
 * This program was prepared by the Regents of the    *
 * University of California at Los Alamos National    *
 * Laboratory (the University) under contract number  *
 * W-7405-ENG-36 with the U.S. Department of Energy   *
 * (DOE).  The University has certain rights in the   *
 * program pursuant to the contract and the program   *
 * should not be copied or distributed outside your   *
 * organization.   All rights in the program are      *
 * reserved by the DOE and the University.  Neither   *
 * the U.S. Government nor the University makes any   *
 * warranty, express or implied, or assumes any       *
 * liability or responsibility for the use of this    *
 * software.                                          *
 *                                                    *
 ******************************************************
    1-       Calculate for hbts, isoksphere
    2-       c cell card
    3-       1 1 -8.96 -1 imp:h,p,n=1
    4-       2 2 -7.0 1 -2 imp:h,p,n=1
    5-       3 3 -0.9777 2 -3 imp:h,p,n=1
    6-       4 4 -11.34 3 -4 imp:h,p,n=1
    7-       5 5 -0.0012 4 -5 imp:h,p,n=1
    8-       6 0 5 imp:h,p,n=0
    9-
   10-       c surface card
   11-       1 sph 0 0 0 0.75
   12-       2 sph 0 0 0 30.75
   13-       3 sph 0 0 0 60.75
   14-       4 sph 0 0 0 64.75
   15-       5 sph 0 0 0 150.75
   16-
   17-       c data card
   18-       c mode card / definition
   19-       mode h p n
   20-       c physics card
   21-       phys:n 70 0 0 0 20 -1 1
   22-       phys:p 70 0 0 1
   23-       phys:e 70 0 0 0 1 0 1 0 1 1
   24-       phys:h 70 0 0 j 0 j 0
   25-       sdef pos=0 0 0 erg=66 par=h
   26-       c material definition
   27-       m1 29063 -1 $ Cu as a source
   28-       m2 26056 -0.89 25000 -0.11 $ cast iron
   29-       m3 6000 -0.83237485 1001 -0.14414685
   30-            5010 -0.0234783
   31-       m4 82208 -1 $ Pb
   32-       m5 7014 -0.7552 8016 -0.232 18040 -0.01280 $ air
   33-       c tallies
```

```
 34-       fM2 6E13
 35-       f2:n 5
 36-       de2 1E-12 2.5E-8 1E-3 1E-2 1E-1 1 10
 37-            30 50 100 200 500 1000 10000
 38-       df2 3.96E-8 4.32E-8 4.68E-8 1.916E-7 1.62E-7 1.044E-6
 39-            2.1204E-6 1.2204E-6 1.4832E-6 1.746E-6 2.0088E-6
 40-            2.502E-6 3.2112E-6 1.098E-5
 41-       de12 0.01 0.02 0.05 0.1 0.5 1
 42-            1.5 2 3 4 5 6
 43-            8 10 20 30 40 50
 44-            100 200 500 1000 10000
 45-       df12 2.232E-10 8.64E-10 1.3248E-9 1.8468E-9 8.928E-9 1.6092E-8
 46-            2.2068E-8 2.6892E-8 3.5784E-8 4.392E-8 4.896E-8 5.472E-8
 47-            6.588E-8 8.028E-8 1.3176E-7 1.8216E-7 2.2356E-7 2.6532E-7
 48-            4.284E-7 5.436E-7 6.84E-7 7.704E-7 1.0548E-6
 49-       fM12 1.07E14
 50-       f12:p 5
 51-       nps 1000000

 warning.  use models for the following missing data tables:
  18040.  c
  25000.  c
   1001.  u
   5010.  u
   6000.  u
   7014.  u
  18040.  u
  25000.  u


1LAHET physics options:                                                                    print table 41

 lca    ielas   ipreq  iexisa  ichoic   jcoul  nexite   npidk   noact    icem
 lca        2       1       1      23       1       1       0       1       0

 lcb    flenb(i),i=1,6                                                        ctofe       flim0
 lcb    3.4900E+03  3.4900E+03  2.4900E+03  2.4900E+03  8.0000E+02  8.0000E+02 -1.0000E+00 -1.0000E+00

 lea     ipht     icc  nobalc  nobale   ifbrk  ilvden   ievap   nofis
 lea        1       4       1       0       1       0       0       1

 leb    yzero       bzero       yzero       bzero
 leb    1.5000E+00  8.0000E+00  1.5000E+00  1.0000E+01

icells                                                                                     print table 60

                      atom        gram                                    neutron     photon      proton       photon wt
       cell  mat     density     density      volume        mass     pieces importance  importance  importance  generation

    1     1    1 8.57426E-02 8.96000E+00 1.76715E+00 1.58336E+01          1 1.0000E+00  1.0000E+00  1.0000E+00  -1.000E+00
    2     2    2 7.55135E-02 7.00000E+00 1.21792E+05 8.52542E+05          1 1.0000E+00  1.0000E+00  1.0000E+00  -1.000E+00
    3     3    3 1.26394E-01 9.77700E-01 8.17340E+05 7.99114E+05          1 1.0000E+00  1.0000E+00  1.0000E+00  -1.000E+00
    4     4    4 3.28354E-02 1.13400E+01 1.97990E+05 2.24521E+06          1 1.0000E+00  1.0000E+00  1.0000E+00  -1.000E+00
    5     5    5 4.96861E-05 1.20000E-03 1.32132E+07 1.58558E+04          1 1.0000E+00  1.0000E+00  1.0000E+00  -1.000E+00
    6     6    0 0.00000E+00 0.00000E+00 0.00000E+00 0.00000E+00          0 0.0000E+00  0.0000E+00  0.0000E+00  -1.000E+00
```

```
total                                    1.43503E+07 3.91274E+06

random number control     0.830205350379520E+14

   minimum source weight = 1.0000E+00    maximum source weight = 1.0000E+00

        1 warning message so far.
1cross-section tables                                                    print table 100

    table    length

                     tables from file endf60

no particle-production data for ipt=  9 from   1001.60c
  1001.60c    2388  1-h-1 from endf-vi.1                                  mat 125      11/25/93
no particle-production data for ipt=  9 from   5010.60c
  5010.60c   24446  5-b-10 from endf-vi.1                                 mat 525      11/25/93
no particle-production data for ipt=  9 from   6000.60c
  6000.60c   19941  6-c-nat from endf-vi.1                                mat 600      11/25/93
no particle-production data for ipt=  9 from   7014.60c
  7014.60c   54936  7-n-14 from special lanl endf-6 evaluation            mat 725      11/25/93
no particle-production data for ipt=  9 from   8016.60c
  8016.60c   54249  8-o-16 from endf/b-vi                        mat 8    25           11/25/93
no particle-production data for ipt=  9 from  26056.60c
 26056.60c  161938  endf/b-vi.1 fe56a                                     mat2631      11/25/93
no particle-production data for ipt=  9 from  29063.60c
 29063.60c  106983  29-cu-63 from endf/b-vi.2                             mat2925      11/27/93
no particle-production data for ipt=  9 from  82208.60c
 82208.60c   59600  endf/b-vi pb208                                      mat8237      11/27/93

                     tables from file mcplib02

  1000.02p     623                                                                   01/15/93
  5000.02p     623                                                                   01/15/93
  6000.02p     623                                                                   01/15/93
  7000.02p     623                                                                   01/15/93
  8000.02p     623                                                                   01/15/93
 18000.02p     643                                                                   01/15/93
 25000.02p     651                                                                   01/15/93
 26000.02p     651                                                                   01/15/93
 29000.02p     663                                                                   01/15/93
 82000.02p     755                                                                   01/15/93

                     tables from file la150u

  8016.24u   72930  LA150 Photonuclear Data Library O-16                  mat 825      07/26/00
 26056.24u   64043  LA150 Photonuclear Data Library Fe-56                 mat2631      07/26/00
 29063.24u   73548  LA150 Photonuclear Data Library Cu-63                 mat2925      07/26/00
 82208.24u   77099  LA150 Photonuclear Data Library Pb-208                mat8237      07/26/00

 total      778579

any neutrons with energy greater than emax = 7.00000E+01 from the source or from a collision will be resampled.

neutron cross sections outside the range from 0.0000E+00 to 7.0000E+01 mev are expunged.
```

maximum photon energy set to 70.0 mev (maximum electron energy)

tables from file e103

1000.03e	2329	6/6/98
5000.03e	2331	6/6/98
6000.03e	2333	6/6/98
7000.03e	2333	6/6/98
8000.03e	2333	6/6/98
18000.03e	2341	6/6/98
25000.03e	2345	6/6/98
26000.03e	2345	6/6/98
29000.03e	2347	6/6/98
82000.03e	2373	6/6/98

1particles and energy limits print table 101

particle type		particle cutoff energy	maximum particle energy	smallest table maximum	largest table maximum	always use table below	always use model above
1	n neutron	0.0000E+00	7.0000E+01	2.0000E+01	7.2000E+01	0.0000E+00	2.0000E+01
2	p photon	1.0000E-03	7.0000E+01	1.0000E+05	1.0000E+05	1.0000E+37	1.0000E+37
	photonuclear	5.7775E+00	7.0000E+01	1.5000E+02	1.5000E+02	0.0000E+00	1.5000E+02
3	e electron	1.0000E-03	7.0000E+01	7.0000E+01	7.0000E+01	1.0000E+37	1.0000E+37
9	h proton	1.0000E+00	7.0000E+01	0.0000E+00	0.0000E+00	0.0000E+00	0.0000E+00

The following nuclides use physics models rather than data tables:

18040.	c
25000.	c
1001.	u
5010.	u
6000.	u
7014.	u
18040.	u
25000.	u

warning. material 1 has been set to a conductor.

warning. material 2 has been set to a conductor.

warning. material 4 has been set to a conductor.

the bremsstrahlung production cross section for all materials is scaled by the factor 0.0000E+00
bremsstrahlung generated on each electron substep.
secondary electron production reduced by 99%.

the knock-on electron production cross section for all materials is scaled by the factor 0.0000E+00

the secondary electron production cross section for all materials is scaled by the factor 1.0000E-02
1decimal words of dynamically allocated storage

```
    general                0
    tallies             6512
    bank               70401
    cross sections    778580

    total                  0    *          0 bytes

************************************************************************************************************************
dump no.    1 on file hbts.r       nps =          0   coll =          0     ctm =   0.00     nrn =          0


       4 warning messages so far.

************************************************************************************************************************
dump no.    2 on file hbts.r       nps =     245440   coll =   83083491     ctm =  15.01     nrn =  489112000


************************************************************************************************************************
dump no.    3 on file hbts.r       nps =     491739   coll =  166450343     ctm =  30.01     nrn =  980001019


************************************************************************************************************************
dump no.    4 on file hbts.r       nps =     737579   coll =  249662329     ctm =  45.02     nrn = 1470052468


************************************************************************************************************************
dump no.    5 on file hbts.r       nps =     983120   coll =  332777503     ctm =  60.03     nrn = 1959657728

1problem summary

     run terminated when   1000000 particle histories were done.
+                                                                                    01/29/06 22:47:34
     Calculate for hbts, iso#sphere                                      probid =  01/29/06 21:46:24

neutron creation       tracks   weight       energy          neutron loss          tracks   weight       energy
                                (per source particle)                                      (per source particle)

source                      0   0.           0.              escape                 441   4.2182E-04   5.9611E-03
nucl. interaction      160193   1.5715E-01   4.7860E-01      energy cutoff            0   0.           0.
particle decay              0   0.           0.              time cutoff              0   0.           0.
weight window               0   0.           0.              weight window            0   0.           0.
cell importance             0   0.           0.              cell importance          0   0.           0.
weight cutoff               0   1.3577E-03   1.1480E-06      weight cutoff        74968   1.3755E-03   1.1832E-06
energy importance           0   0.           0.              energy importance        0   0.           0.
dxtran                      0   0.           0.              dxtran                   0   0.           0.
forced collisions           0   0.           0.              forced collisions        0   0.           0.
exp. transform              0   0.           0.              exp. transform           0   0.           0.
upscattering                0   0.           4.7671E-10      downscattering           0   0.           1.9050E-01
photonuclear               27   1.2507E-09   2.3644E-09      capture                  0   7.6431E-02   1.1807E-02
(n,xn)                   3620   3.3182E-03   5.7383E-03      loss to (n,xn)        1807   1.6563E-03   2.7170E-02
prompt fission              0   0.           0.              loss to fission          0   0.           0.
delayed fission             0   0.           0.              nucl. interaction    86624   8.1943E-02   2.4890E-01
                                                             particle decay           0   0.           0.
tabular boundary        58463   5.5047E-02   3.9872E-02      tabular boundary     58463   5.5047E-02   3.9872E-02
tabular sampling            0   0.           0.
    total              222303   2.1688E-01   5.2421E-01          total           222303   2.1688E-01   5.2421E-01
```

number of neutrons banked	220496	average time of (shakes)		cutoffs	
neutron tracks per source particle	2.2230E-01	escape	7.4277E+01	tco	1.0000E+34
neutron collisions per source particle	3.2688E+00	capture	2.2564E+02	eco	0.0000E+00
total neutron collisions	3268793	capture or escape	2.2481E+02	wc1	-5.0000E-01
net multiplication	0.0000E+00 0.0000	any termination	1.3972E+02	wc2	-2.5000E-01

photon creation	tracks	weight (per source particle)	energy	photon loss	tracks	weight (per source particle)	energy
source	0	0.	0.	escape	290	2.7130E-04	7.4995E-04
nucl. interaction	237939	2.2972E-01	3.0137E-01	energy cutoff	0	0.	0.
particle decay	0	0.	0.	time cutoff	0	0.	0.
weight window	0	0.	0.	weight window	0	0.	0.
cell importance	0	0.	0.	cell importance	0	0.	0.
weight cutoff	0	0.	0.	weight cutoff	0	0.	0.
energy importance	0	0.	0.	energy importance	0	0.	0.
dxtran	0	0.	0.	dxtran	0	0.	0.
forced collisions	0	0.	0.	forced collisions	0	0.	0.
exp. transform	0	0.	0.	exp. transform	0	0.	0.
from neutrons	171655	1.7596E-01	2.1617E-01	compton scatter	0	0.	3.9366E-01
bremsstrahlung	0	0.	0.	capture	513353	5.0846E-01	5.3497E-02
p-annihilation	306	3.1056E-04	1.5870E-04	pair production	15334	1.5202E-02	7.1270E-02
photonuclear	8	2.0022E-06	7.7483E-06	photonuclear abs	0	1.0622E-06	9.5119E-06
electron x-rays	0	0.	0.				
1st fluorescence	116101	1.1500E-01	1.4431E-03				
2nd fluorescence	2968	2.9407E-03	3.5926E-05				
(gamma,xgamma)	0	0.	0.				
tabular sampling	0	0.	0.				
total	528977	5.2394E-01	5.1918E-01	total	528977	5.2394E-01	5.1918E-01

number of photons banked	412723	average time of (shakes)		cutoffs	
photon tracks per source particle	5.2898E-01	escape	7.5609E+02	tco	1.0000E+34
photon collisions per source particle	2.4345E+00	capture	1.5432E+09	eco	1.0000E-03
total photon collisions	2434451	capture or escape	1.5424E+09	wc1	-5.0000E-01
		any termination	1.4977E+09	wc2	-2.5000E-01

proton creation	tracks	weight (per source particle)	energy	proton loss	tracks	weight (per source particle)	energy
source	1000000	1.0000E+00	6.5000E+01	escape	0	0.	0.
nucl. interaction	73668	7.3666E-02	7.9335E-01	energy cutoff	1024025	1.0237E+00	1.0237E+00
particle decay	0	0.	0.	time cutoff	0	0.	0.
weight window	0	0.	0.	weight window	0	0.	0.
cell importance	0	0.	0.	cell importance	0	0.	0.
weight cutoff	0	0.	0.	weight cutoff	0	0.	0.
energy importance	0	0.	0.	energy importance	0	0.	0.
dxtran	0	0.	0.	dxtran	0	0.	0.
forced collisions	0	0.	0.	forced collisions	0	0.	0.
exp. transform	0	0.	0.	exp. transform	0	0.	0.
tabular sampling	0	0.	0.	multiple scatter	0	0.	6.3510E+01
				bremsstrahlung	0	0.	0.
photonuclear	0	0.	0.	nucl. interaction	54035	5.4035E-02	2.2682E+00
elastic recoil	4343	4.1075E-03	1.4318E-02	elastic scatter	0	0.	6.0285E-03
				particle decay	0	0.	0.
				capture	0	0.	0.

(gamma,xgen_chg)	49	8.6232E-08	2.7440E-07	tabular sampling	0	0.	0.
total	1078060	1.0778E+00	6.6808E+01	total	1078060	1.0778E+00	6.6808E+01

number of particles banked	78060	cutoffs	
particle tracks per source particle	1.0781E+00	tco	1.0000E+34
particle substeps per source particle	3.3279E+02	eco	1.0000E+00
total particle substeps	332785807	wc1	0.0000E+00
		wc2	0.0000E+00

computer time so far in this run	61.16 minutes	maximum number ever in bank	22
computer time in mcrun	61.06 minutes	bank overflows to backup file	0
source particles per minute	1.6377E+04	dynamic storage	0 words, 0 bytes.
random numbers generated	1993243282	most random numbers used was	29316 in history 108473

range of sampled source weights = 1.0000E+00 to 1.0000E+00

1neutron activity in each cell print table 126

	cell	tracks entering	population	collisions	collisions * weight (per history)	number weighted energy	flux weighted energy	average track weight (relative)	average track mfp (cm)
1	1	3039	73364	17328	1.7280E-02	1.3457E+00	4.7207E+00	9.9753E-01	3.3880E+00
2	2	104034	219502	2236324	1.9784E+00	2.1414E-02	9.9383E-01	9.4172E-01	8.8422E+00
3	3	101476	81970	1014355	9.6204E-01	3.3550E-03	1.0247E+00	9.5388E-01	1.2111E+00
4	4	450	583	782	7.3515E-04	1.1954E-01	9.4258E+00	9.5056E-01	5.3090E+00
5	5	441	441	4	3.7816E-06	3.0505E-01	1.3246E+01	9.5600E-01	1.1838E+04
total		209440	375860	3268793	2.9584E+00				

1photon activity in each cell print table 126

	cell	tracks entering	population	collisions	collisions * weight (per history)	number weighted energy	flux weighted energy	average track weight (relative)	average track mfp (cm)
1	1	5865	143187	87244	8.7512E-02	1.5764E+00	1.5764E+00	1.0034E+00	2.0043E+00
2	2	161807	357158	1749257	1.7398E+00	1.0778E+00	1.0778E+00	9.9627E-01	2.0186E+00
3	3	15016	70883	550365	5.4723E-01	2.6436E-01	2.6436E-01	9.9335E-01	7.2368E+00
4	4	22252	24700	47583	4.7061E-02	1.5900E+00	1.5900E+00	9.6857E-01	1.0279E+00
5	5	290	290	2	1.9949E-06	2.7004E+00	2.7004E+00	9.3803E-01	2.0596E+04
total		205230	596218	2434451	2.4216E+00				

1proton activity in each cell print table 126

	cell	tracks entering	population	substeps	substeps * weight (per history)	number weighted energy	flux weighted energy	average track weight (relative)	average track mfp (cm)
1	1	1000000	1071101	332310313	3.3231E+02	3.7373E+01	4.2439E+01	1.0000E+00	7.0281E-03
2	2	8	2586	345091	3.4476E-01	1.0037E+01	1.3308E+01	9.9962E-01	1.6009E-03
3	3	0	4380	128015	1.2034E-01	9.3030E+00	1.3063E+01	9.6576E-01	1.3681E-02
4	4	6	7	2388	2.3055E-03	7.9585E+00	9.3522E+00	9.9002E-01	3.4434E-04
5	5	0	0	0	0.0000E+00	0.0000E+00	0.0000E+00	0.0000E+00	0.0000E+00
total		1000014	1078074	332785807	3.3277E+02				

1summary of protons produced in neutron collisions

	cell	number of photons	weight per source neut	energy per source neut	avg photon energy	mev/gm per source neut	weight/neut collision	energy/neut collision
1	1	5224	5.64453E-03	8.59200E-03	1.52218E+00	5.42642E-04	3.26648E-01	4.97218E-01
2	2	102105	1.05980E-01	1.75536E-01	1.65631E+00	2.05897E-07	5.35690E-02	8.87267E-02
3	3	64183	6.41830E-02	3.17623E-02	4.94871E-01	3.97469E-08	6.67152E-02	3.30154E-02
4	4	143	1.54229E-04	2.77874E-04	1.80169E+00	1.23763E-10	2.09792E-01	3.77982E-01
5	5	0	0.00000E+00	0.00000E+00	0.00000E+00	0.00000E+00	0.00000E+00	0.00000E+00
6	6	0	0.00000E+00	0.00000E+00	0.00000E+00	0.00000E+00	0.00000E+00	0.00000E+00
	total	171655	1.75962E-01	2.16168E-01	1.22849E+00			

energy interval	number of photons	number frequency	cum number distribution	weight of photons	weight frequency	cum weight distribution
20.000	0	0.00000E+00	0.00000E+00	0.00000E+00	0.00000E+00	0.00000E+00
15.000	3	1.74769E-05	1.74769E-05	3.23296E-06	1.83731E-05	1.83731E-05
10.000	21	1.22338E-04	1.39815E-04	2.52953E-05	1.43754E-04	1.62127E-04
9.000	364	2.12053E-03	2.26035E-03	3.73755E-04	2.12406E-03	2.28619E-03
8.000	324	1.88751E-03	4.14785E-03	3.51416E-04	1.99711E-03	4.28330E-03
7.000	3517	2.04888E-02	2.46366E-02	3.66882E-03	2.08501E-02	2.51334E-02
6.000	1198	6.97912E-03	3.16157E-02	1.32727E-03	7.54295E-03	3.26763E-02
5.000	1711	9.96767E-03	4.15834E-02	1.89393E-03	1.07633E-02	4.34396E-02
4.000	2902	1.69060E-02	5.84894E-02	3.20727E-03	1.82271E-02	6.16667E-02
3.000	4989	2.90641E-02	8.75535E-02	5.40464E-03	3.07149E-02	9.23816E-02
2.000	8538	4.97393E-02	1.37293E-01	9.01369E-03	5.12252E-02	1.43607E-01
1.000	15411	8.97789E-02	2.27072E-01	1.64649E-02	9.35706E-02	2.37177E-01
0.500	61734	3.59640E-01	5.86712E-01	6.28532E-02	3.57198E-01	5.94375E-01
0.100	66451	3.87120E-01	9.73831E-01	6.66770E-02	3.78929E-01	9.73304E-01
0.010	3749	2.18403E-02	9.95672E-01	3.93593E-03	2.23681E-02	9.95672E-01
0.000	743	4.32845E-03	1.00000E+00	7.61548E-04	4.32791E-03	1.00000E+00
total	171655	1.00000E+00		1.75962E-01	1.00000E+00	

```
1tally   2        nps =  1000000
          tally type 2    particle flux averaged over a surface.
          particle(s): neutron

          this tally is modified by a dose function.

          this tally is all multiplied by  6.00000E+13

          areas
               surface:        5
                       2.85578E+05

 surface  5
                1.14486E-01 0.0574
1analysis of the results in the tally fluctuation chart bin (tfc) for tally   2 with nps =   1000000    print table 160


 normed average tally per history  = 1.14486E-01          unnormed average tally per history  = 3.26947E+04
 estimated tally relative error    = 0.0574               estimated variance of the variance  = 0.0069
 relative error from zero tallies  = 0.0521               relative error from nonzero scores  = 0.0241

 number of nonzero history tallies =         368          efficiency for the nonzero tallies  = 0.0004
```

history number of largest tally = 969713 largest unnormalized history tally = 4.11325E+08
(largest tally)/(average tally) = 1.25808E+04 (largest tally)/(avg nonzero tally)= 4.62973E+00

(confidence interval shift)/mean = 0.0021 shifted confidence interval center = 1.14721E-01

if the largest history score sampled so far were to occur on the next history, the tfc bin quantities would change as follows:

estimated quantities	value at nps	value at nps+1	value(nps+1)/value(nps)-1.
mean	1.14486E-01	1.15926E-01	0.012580
relative error	5.74207E-02	5.80522E-02	0.010998
variance of the variance	6.90263E-03	8.38219E-03	0.214347
shifted center	1.14721E-01	1.14743E-01	0.000194
figure of merit	4.96697E+00	4.85949E+00	-0.021638

there is not enough information in the largest history scores (usually less than 500 scores) for a reliable estimate of the slope.
the history score probability density function appears to have an unsampled region at the largest history scores: please examine.

results of 10 statistical checks for the estimated answer for the tally fluctuation chart (tfc) bin of tally 2

tfc bin	--mean--	---------relative error---------			----variance of the variance----			--figure of merit--		-pdf-
behavior	behavior	value	decrease	decrease rate	value	decrease	decrease rate	value	behavior	slope
desired	random	<0.10	yes	1/sqrt(nps)	<0.10	yes	1/nps	constant	random	>3.00
observed	random	0.06	yes	yes	0.01	yes	yes	constant	random	0.00
passed?	yes	yes	yes	yes	yes	yes	yes	yes	yes	no

warning. the tally in the tally fluctuation chart bin did not pass 1 of the 10 statistical checks.

fom = (histories/minute)*(f(x) signal-to-noise ratio)**2 = (1.638E+04)*(1.742E-02)**2 = (1.638E+04)*(3.033E-04) = 4.967E+00
unnormed tally density for tally 2 nonzero tally mean(m) = 8.884E+07 nps = 1000000 print table 161

abscissa	ordinate	log plot of tally probability density function in tally fluctuation chart bin(d=decade,slope= 0.0)
tally	number num den log den	d----------d----------d----------
2.51+06	3 5.81-12 -11.236	********** | ********** | **********
3.16+06	3 4.61-12 -11.336	********** | ********** | **********
3.98+06	0 0.00+00 0.000	| |
5.01+06	0 0.00+00 0.000	| |
6.31+06	2 1.54-12 -11.812	********** | ********** | ********
7.94+06	1 6.12-13 -12.213	********** | ********** |
1.00+07	4 1.94-12 -11.711	********** | ********** | **********
1.26+07	6 2.32-12 -11.635	********** | ********** | **********
1.58+07	2 6.14-13 -12.212	********** | ********** |
2.00+07	3 7.31-13 -12.136	********** | ********** |
2.51+07	2 3.87-13 -12.412	********** | ********** |
3.16+07	2 3.08-13 -12.512	********** | ********** |
3.98+07	3 3.66-13 -12.436	********** | ********** |
5.01+07	3 2.91-13 -12.536	********** | ********** |
6.31+07	11 8.48-13 -12.072	********** | ********** |

```
7.94+07     80 4.90-12 -11.310 *********************************|*********************************|************************
1.00+08    150 7.29-12 -11.137 *********************************|*********************************|*********************************
1.26+08     59 2.28-12 -11.642 *********************************|*********************************|**************
1.58+08     16 4.91-13 -12.309 *********************************|*************************        |
2.00+08      9 2.19-13 -12.659 *********************************|**************                   |
2.51+08      7 1.35-13 -12.868 *********************************|******                           |
3.16+08      1 1.54-14 -13.813 ********                         |                                 |
3.98+08      0 0.00+00   0.000                                  |                                 |
5.01+08      1 9.70-15 -14.013 *                                |                                 |
 total     368 3.68-04         d--------------------------------d---------------------------------d---------------------------------


cumulative tally number for tally   2          nonzero tally mean(m) = 8.884E+07    nps =    1000000     print table 162

  abscissa      cum    ordinate    plot of the cumulative number of tallies in the tally fluctuation chart bin from 0 to 100 percent
   tally       number  cum pct:---------10--------20--------30--------40--------50--------60--------70--------80--------90-------100
2.51189E+06       3     0.815|*        |         |         |         |         |         |         |         |         |         |
3.16228E+06       6     1.630|**       |         |         |         |         |         |         |         |         |         |
3.98108E+06       6     1.630|**       |         |         |         |         |         |         |         |         |         |
5.01188E+06       6     1.630|**       |         |         |         |         |         |         |         |         |         |
6.30958E+06       8     2.174|**       |         |         |         |         |         |         |         |         |         |
7.94329E+06       9     2.446|**       |         |         |         |         |         |         |         |         |         |
1.00000E+07      13     3.533|****     |         |         |         |         |         |         |         |         |         |
1.25893E+07      19     5.163|*****    |         |         |         |         |         |         |         |         |         |
1.58490E+07      21     5.707|******   |         |         |         |         |         |         |         |         |         |
1.99526E+07      24     6.522|*******  |         |         |         |         |         |         |         |         |         |
2.51189E+07      26     7.065|*******  |         |         |         |         |         |         |         |         |         |
3.16228E+07      28     7.609|******** |         |         |         |         |         |         |         |         |         |
3.98108E+07      31     8.424|******** |         |         |         |         |         |         |         |         |         |
5.01188E+07      34     9.239|*********|         |         |         |         |         |         |         |         |         |
6.30958E+07      45    12.228|*********|**       |         |         |         |         |         |         |         |         |
7.94329E+07     125    33.967|*********|*********|*********|****     |         |         |         |         |         |         |
1.00000E+08     275    74.728|*********|*********|*********|*********|*********|*********|*********|*****    |         |         |
1.25893E+08     334    90.761|*********|*********|*********|*********|*********|*********|*********|*********|*********|*        |
1.58490E+08     350    95.109|*********|*********|*********|*********|*********|*********|*********|*********|*********|*****    |
1.99526E+08     359    97.554|*********|*********|*********|*********|*********|*********|*********|*********|*********|******** |
2.51189E+08     366    99.457|*********|*********|*********|*********|*********|*********|*********|*********|*********|*********|
3.16228E+08     367    99.728|*********|*********|*********|*********|*********|*********|*********|*********|*********|*********|
3.98108E+08     367    99.728|*********|*********|*********|*********|*********|*********|*********|*********|*********|*********|
5.01188E+08     368   100.000|*********|*********|*********|*********|*********|*********|*********|*********|*********|*********|
   total        368   100.000:---------10--------20--------30--------40--------50--------60--------70--------80--------90-------100
1tally  12         nps =   1000000
           tally type 2    particle flux averaged over a surface.
           particle(s): photon


           this tally is modified by a dose function.


           this tally is all multiplied by  1.07000E+14


           areas
               surface:          5
                          2.85578E+05


 surface  5
                3.23414E-03 0.0679
1analysis of the results in the tally fluctuation chart bin (tfc) for tally  12 with nps =   1000000     print table 160
```

```
normed average tally per history  = 3.23414E-03        unnormed average tally per history  = 9.23598E+02
estimated tally relative error    = 0.0679            estimated variance of the variance  = 0.0086
relative error from zero tallies  = 0.0591            relative error from nonzero scores  = 0.0334

number of nonzero history tallies =        286        efficiency for the nonzero tallies  = 0.0003
history number of largest  tally  =     965329        largest  unnormalized history tally = 1.34960E+07
(largest  tally)/(average tally)  = 1.46124E+04       (largest  tally)/(avg nonzero tally)= 4.17915E+00

(confidence interval shift)/mean  = 0.0029            shifted confidence interval center  = 3.24339E-03
```

if the largest history score sampled so far were to occur on the next history, the tfc bin quantities would change as follows:

estimated quantities	value at nps	value at nps+1	value(nps+1)/value(nps)-1.
mean	3.23414E-03	3.28139E-03	0.014611
relative error	6.79206E-02	6.84739E-02	0.008146
variance of the variance	8.63799E-03	9.84703E-03	0.139967
shifted center	3.24339E-03	3.24403E-03	0.000196
figure of merit	3.54997E+00	3.49283E+00	-0.016095

there is not enough information in the largest history scores (usually less than 500 scores) for a reliable estimate of the slope.
the history score probability density function appears to have an unsampled region at the largest history scores: please examine.

results of 10 statistical checks for the estimated answer for the tally fluctuation chart (tfc) bin of tally 12

tfc bin	--mean--	----------relative error----------			----variance of the variance----			--figure of merit--		-pdf-
behavior	behavior	value	decrease	decrease rate	value	decrease	decrease rate	value	behavior	slope
desired	random	<0.10	yes	1/sqrt(nps)	<0.10	yes	1/nps	constant	random	>3.00
observed	random	0.07	yes	yes	0.01	yes	yes	constant	random	0.00
passed?	yes	yes	yes	yes	yes	yes	yes	yes	yes	no

warning. the tally in the tally fluctuation chart bin did not pass 1 of the 10 statistical checks.

fom = (histories/minute)*(f(x) signal-to-noise ratio)**2 = (1.638E+04)*(1.472E-02)**2 = (1.638E+04)*(2.168E-04) = 3.550E+00

1unnormed tally density for tally 12 nonzero tally mean(m) = 3.229E+06 nps = 1000000 print table 161

```
abscissa              ordinate   log plot of tally probability density function in tally fluctuation chart bin(d=decade,slope= 0.0)
 tally  number num den log den:d----------d----------d----------
2.00+05      1 2.44-11 -10.613 **********|**********                |
2.51+05      0 0.00+00   0.000           |                          |
3.16+05      1 1.54-11 -10.813 **********|**********                |
3.98+05      0 0.00+00   0.000           |                          |
5.01+05      0 0.00+00   0.000           |                          |
6.31+05      0 0.00+00   0.000           |                          |
7.94+05      5 3.06-11 -10.514 **********|**********                |
1.00+06     14 6.81-11 -10.167 **********|**********|***************
```

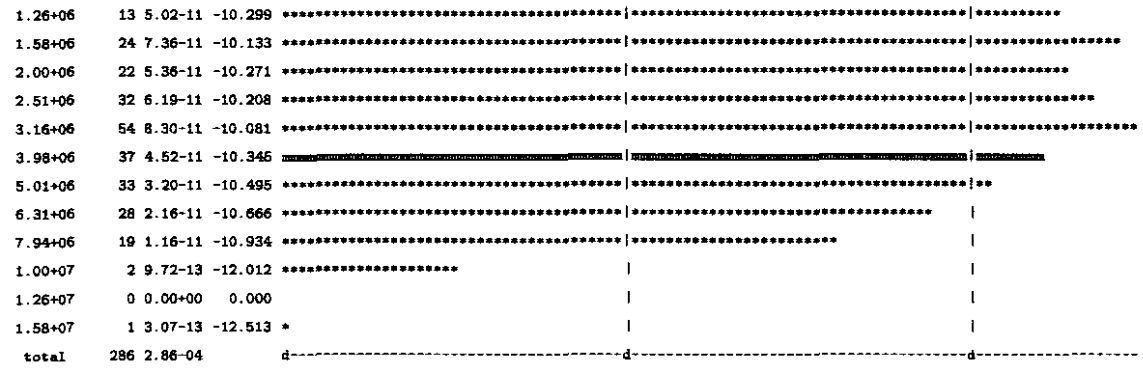

1.26+06	13	5.02-11	-10.299	
1.58+06	24	7.36-11	-10.133	
2.00+06	22	5.36-11	-10.271	
2.51+06	32	6.19-11	-10.208	
3.16+06	54	8.30-11	-10.081	
3.98+06	37	4.52-11	-10.345	
5.01+06	33	3.20-11	-10.495	
6.31+06	28	2.16-11	-10.666	
7.94+06	19	1.16-11	-10.934	
1.00+07	2	9.72-13	-12.012	
1.26+07	0	0.00+00	0.000	
1.58+07	1	3.07-13	-12.513	
total	286	2.86-04		

cumulative tally number for tally 12 nonzero tally mean(m) = 3.229E+06 nps = 1000000 print table 162

abscissa tally	cum number	ordinate cum pct	plot of the cumulative number of tallies in the tally fluctuation chart bin from 0 to 100 percent
			:--------10--------20--------30--------40--------50--------60--------70--------80--------90-------100
1.99526E+05	1	0.350	
2.51189E+05	1	0.350	
3.16228E+05	2	0.699	*
3.98108E+05	2	0.699	*
5.01188E+05	2	0.699	*
6.30958E+05	2	0.699	*
7.94329E+05	7	2.448	**
1.00000E+06	21	7.343	*******
1.25893E+06	34	11.888	**********|**
1.58490E+06	58	20.280	**********|**********
1.99526E+06	80	27.972	**********|**********|********
2.51189E+06	112	39.161	**********|**********|**********|**********
3.16228E+06	166	58.042	**********|**********|**********|**********|**********|********
3.98108E+06	203	70.979	
5.01188E+06	236	82.517	**********|**********|**********|**********|**********|**********|**********|**********|***
6.30958E+06	264	92.308	**********|**********|**********|**********|**********|**********|**********|**********|**********|**
7.94329E+06	283	98.951	**********|**********|**********|**********|**********|**********|**********|**********|**********|**********
1.00000E+07	285	99.650	**********|**********|**********|**********|**********|**********|**********|**********|**********|**********
1.25893E+07	285	99.650	**********|**********|**********|**********|**********|**********|**********|**********|**********|**********
1.58490E+07	286	100.000	**********|**********|**********|**********|**********|**********|**********|**********|**********|**********
total	286	100.000	:--------10--------20--------30--------40--------50--------60--------70--------80--------90-------100

1status of the statistical checks used to form confidence intervals for the mean for each tally bin

tally result of statistical checks for the tfc bin (the first check not passed is listed) and error magnitude check for all bins

2 missed 1 of 10 tfc bin checks: there is insufficient tfc bin tally information to estimate the large tally slope reliably
passed all bin error check: 1 tally bins all have relative errors less than 0.10 with no zero bins

12 missed 1 of 10 tfc bin checks: there is insufficient tfc bin tally information to estimate the large tally slope reliably
passed all bin error check: 1 tally bins all have relative errors less than 0.10 with no zero bins

the 10 statistical checks are only for the tally fluctuation chart bin and do not apply to other tally bins.

warning. 2 of the 2 tally fluctuation chart bins did not pass all 10 statistical checks.

1tally fluctuation charts

	tally 2					tally 12				
nps	mean	error	vov	slope	fom	mean	error	vov	slope	fom
64000	7.5601E-02	0.2636	0.0839	0.0	3.7E+00	3.7692E-03	0.2453	0.0906	0.0	4.3E+00
128000	7.8377E-02	0.1875	0.0475	0.0	3.6E+00	3.0991E-03	0.1846	0.0508	0.0	3.8E+00
192000	8.9909E-02	0.1444	0.0335	0.0	4.1E+00	3.2563E-03	0.1569	0.0374	0.0	3.5E+00
256000	9.3443E-02	0.1204	0.0220	0.0	4.4E+00	3.2539E-03	0.1351	0.0274	0.0	3.5E+00
320000	9.7041E-02	0.1041	0.0158	0.0	4.7E+00	3.2861E-03	0.1201	0.0217	0.0	3.5E+00
384000	9.8594E-02	0.0961	0.0139	0.0	4.6E+00	3.0985E-03	0.1114	0.0189	0.0	3.4E+00
448000	1.0410E-01	0.0876	0.0116	0.0	4.8E+00	3.3083E-03	0.1003	0.0155	0.0	3.6E+00
512000	1.0369E-01	0.0819	0.0101	0.0	4.8E+00	3.2380E-03	0.0952	0.0139	0.0	3.5E+00
576000	1.0220E-01	0.0776	0.0089	0.0	4.7E+00	3.1485E-03	0.0907	0.0127	0.0	3.5E+00
640000	1.0570E-01	0.0731	0.0084	0.0	4.8E+00	3.1901E-03	0.0859	0.0115	0.0	3.5E+00
704000	1.0454E-01	0.0699	0.0077	0.0	4.8E+00	3.1484E-03	0.0819	0.0106	0.0	3.5E+00
768000	1.0595E-01	0.0665	0.0069	0.0	4.8E+00	3.2167E-03	0.0776	0.0094	0.0	3.5E+00
832000	1.0578E-01	0.0641	0.0064	0.0	4.8E+00	3.1865E-03	0.0743	0.0088	0.0	3.6E+00
896000	1.0762E-01	0.0615	0.0060	0.0	4.8E+00	3.1858E-03	0.0715	0.0081	0.0	3.6E+00
960000	1.1117E-01	0.0582	0.0052	0.0	5.0E+00	3.1915E-03	0.0687	0.0074	0.0	3.6E+00
1000000	1.1449E-01	0.0574	0.0069	0.0	5.0E+00	3.2341E-03	0.0679	0.0086	0.0	3.5E+00

****

dump no. 6 on file hbts.r nps = 1000000 coll = 338489051 ctm = 61.06 nrn = 1993243282

7 warning messages so far.

run terminated when 1000000 particle histories were done.

computer time = 61.16 minutes

mcnpx version 2.5e Mon Feb 23 08:00:00 MST 2004 01/29/06 22:47:34 probid = 01/29/06 21:46:24

Chapter 7

APPENDIX B - Calculated neutron and photon dose rates

The neutron and photon dose rate values calculated in this study are presented in the tables below. The data is categorized under isotropic and anisotropic source terms. In order to obtain the dose attenuation factors of each material equation (3.21) was used. The dose rate without shielding is given separately in Table 7.1 below. Note that the for anisotropic source terms the values represented in this study are those values obtained when the spherical geometry was modeled.

7.1 Isotropic source terms

Tables 7.2, to 7.7 give the values obtained from the determination of (a) boron carbide mixing percentage, (b) depth of iron with respect to iron/wax shield, and (c) the position of iron/wax with respect to iron/wax/iron shield, respectively.

Geometry (cm)	Source (cm)	Dose rate (Sv/hr × particle/cm^2)	
		Neutron	Photons
Spherical	Isotropic	1.74 ×10	9.56×10^{-1}
	Anisotropic	1.51 ×10	7.87×10^{-1}
Cylindrical	Isotropic	1.38 ×10	7.53×10^{-1}

Table 7.1: Neutron and photon dose rates calculated at 1.5 m from centre of source without shielding.

7.1.1 spherical geometry

Tables 7.2 to 7.4 shows the values obtained for this geometry.

Weight percent	Dose rate (Sv/hr × particle/cm^2)	
	Neutron	Photons
0%	5.22×10^{-3}	1.26×10^{-2}
0.5%	4.78×10^{-3}	1.81×10^{-3}
1%	4.29×10^{-3}	1.42×10^{-3}
1.5%	4.46×10^{-3}	1.27×10^{-3}
2%	4.46×10^{-3}	1.15×10^{-3}
2.5%	4.59×10^{-3}	1.01×10^{-3}
3%	4.57×10^{-3}	9.82×10^{-4}
4%	4.61×10^{-3}	8.74×10^{-4}
5%	4.36×10^{-3}	7.96×10^{-4}
6%	4.48×10^{-3}	7.79×10^{-4}
7%	4.55×10^{-3}	7.98×10^{-4}
8%	4.49×10^{-3}	7.09×10^{-4}

Table 7.2: Neutron and photon dose rate calculated at 1.5 m from centre of source for a 60 cm thick iron/wax/lead spherical geometry, as function of boron carbide mixing ratio.

Fe thickness (cm)	Wax thickness (cm)	Dose rate (Sv/hr × particle/cm^2)	
		Neutron	Photons
0	60	3.61×10^{-1}	1.94×10^{-1}
10	50	2.60×10^{-1}	7.17×10^{-2}
20	40	1.71×10^{-1}	4.40×10^{-2}
30	30	1.20×10^{-1}	4.49×10^{-2}
40	20	7.90×10^{-2}	5.74×10^{-2}
41	19	7.39×10^{-2}	5.93×10^{-2}
42	18	6.47×10^{-2}	6.16×10^{-2}
43	17	6.95×10^{-2}	5.93×10^{-2}
44	16	6.30×10^{-2}	6.51×10^{-2}
45	15	6.81×10^{-2}	6.85×10^{-2}
46	14	6.67×10^{-2}	7.02×10^{-2}
47	13	6.97×10^{-2}	7.26×10^{-2}

Table 7.3: Neutron and photon dose rate calculated at 1.5 m from centre of source for a 60 cm thick iron/wax spherical geometry, as function of iron depth.

Fe (cm)	Wax (cm)	Fe (cm)	Dose rate (Sv/hr × particle/cm^2)	
			Neutron	Photons
0	20	40	5.95×10^{-1}	3.29×10^{-3}
10	20	30	3.25×10^{-1}	2.42×10^{-3}
20	20	20	2.12×10^{-1}	2.54×10^{-3}
30	20	10	1.35×10^{-1}	5.06×10^{-3}
40	20	0	7.90×10^{-2}	5.74×10^{-2}

Table 7.4: Neutron and photon dose rate calculated at 1.5 m from centre of source for a 60 cm thick iron/wax/iron spherical geometry, as function of iron/wax depth.

7.1.2 cylindrical geometry

Tables 7.5 to 7.7 show the values obtained for this geometry.

Weight percent	Dose rate (Sv/hr × particle/cm^2)	
	Neutron	Photons
0%	3.33×10^{-3}	1.02×10^{-2}
0.5%	2.92×10^{-3}	1.55×10^{-3}
1%	3.01×10^{-3}	1.29×10^{-3}
1.5%	2.99×10^{-3}	1.11×10^{-3}
2%	3.09×10^{-3}	9.55×10^{-4}
2.5%	2.87×10^{-3}	8.47×10^{-4}
3%	2.68×10^{-3}	7.77×10^{-4}
4%	2.57×10^{-3}	6.57×10^{-4}
5%	2.64×10^{-3}	5.69×10^{-4}
6%	2.85×10^{-3}	5.26×10^{-4}
7%	3.05×10^{-3}	5.40×10^{-4}
8%	3.05×10^{-3}	4.75×10^{-4}

Table 7.5: Neutron and photon dose rate calculated at 1.5 m from centre of source for a 60 cm thick iron/wax/lead cylindrical geometry, as function of boron carbide mixing ratio.

Fe thickness (cm)	Wax thickness (cm)	Dose rate (Sv/hr × particle/cm^2)	
		Neutron	Photons
0	60	2.14×10^{-1}	1.26×10^{-1}
10	50	1.51×10^{-1}	4.31×10^{-2}
20	40	9.79×10^{-2}	2.62×10^{-2}
30	30	7.18×10^{-2}	2.95×10^{-2}
40	20	3.54×10^{-2}	3.99×10^{-2}
41	19	3.40×10^{-2}	4.17×10^{-2}
42	18	3.54×10^{-2}	4.36×10^{-2}
43	17	3.66×10^{-2}	4.41×10^{-2}
44	16	3.22×10^{-2}	4.64×10^{-2}
45	15	3.41×10^{-2}	4.78×10^{-2}
46	14	3.39×10^{-2}	5.00×10^{-2}
47	13	3.51×10^{-2}	5.28×10^{-2}

Table 7.6: Neutron and photon dose rate calculated at 1.5 m from centre of source for a 60 cm thick iron/wax cylindrical geometry, as function of iron depth.

Fe (cm)	Wax (cm)	Fe (cm)	Dose rate (Sv/hr × particle/cm^2)	
			Neutron	Photons
0	20	40	3.49×10^{-1}	2.36×10^{-3}
10	20	30	1.90×10^{-1}	1.31×10^{-3}
20	20	20	1.15×10^{-1}	1.23×10^{-3}
30	20	10	6.89×10^{-2}	2.89×10^{-3}
40	20	0	3.54×10^{-2}	3.99×10^{-2}

Table 7.7: Neutron and photon dose rate calculated at 1.5 m from centre of source for a 60 cm thick iron/wax/iron cylindrical geometry, as function of iron/wax depth.

7.2 Anisotropic

Similarly, the values of dose attenuation factor as a function of (a) boron carbide, (b) iron thickness, and (c) iron/wax interface are respectively given in Tables 7.8 and 7.10 below.

Weight percent	Dose rate (Sv/hr × particle/cm^2)	
	Neutron	Photons
0%	5.85×10^{-3}	1.56×10^{-2}
0.5%	5.69×10^{-3}	2.76×10^{-3}
1%	5.90×10^{-3}	2.14×10^{-3}
1.5%	5.76×10^{-3}	2.14×10^{-3}
2%	5.41×10^{-3}	1.71×10^{-3}
2.5%	5.49×10^{-3}	1.68×10^{-3}
3%	5.29×10^{-3}	1.44×10^{-3}
4%	5.25×10^{-3}	1.33×10^{-3}
5%	5.44×10^{-3}	1.29×10^{-3}
6%	5.08×10^{-3}	1.17×10^{-3}
7%	5.02×10^{-3}	1.16×10^{-3}
8%	5.18×10^{-3}	1.06×10^{-3}

Table 7.8: Neutron and photon dose rate calculated at 1.5 m from centre of source for a 60 cm thick iron/wax/lead spherical geometry, as function of boron carbide mixing ratio.

Fe thickness (cm)	Wax thickness (cm)	Dose rate (Sv/hr × particle/cm^2)	
		Neutron	Photons
0	60	3.52×10^{-1}	1.68×10^{-1}
10	50	2.43×10^{-1}	7.37×10^{-2}
20	40	1.67×10^{-1}	4.31×10^{-2}
30	30	1.12×10^{-1}	4.50×10^{-2}
40	20	8.24×10^{-2}	5.71×10^{-2}
41	19	8.16×10^{-2}	5.96×10^{-2}
42	18	7.62×10^{-2}	6.23×10^{-2}
43	17	7.64×10^{-2}	6.43×10^{-2}
44	16	7.03×10^{-2}	6.68×10^{-2}
45	15	6.99×10^{-2}	6.86×10^{-2}
46	14	6.75×10^{-2}	7.19×10^{-2}
47	13	6.88×10^{-2}	7.35×10^{-2}

Table 7.9: Neutron and photon dose rate calculated at 1.5 m from centre of source for a 60 cm thick iron/wax spherical geometry, as function of iron depth.

Fe (cm)	Wax (cm)	Fe (cm)	Dose rate (Sv/hr × particle/cm^2)	
			Neutron	Photons
0	20	40	5.63×10^{-1}	2.90×10^{-3}
10	20	30	3.11×10^{-1}	2.12×10^{-3}
20	20	20	1.83×10^{-1}	2.54×10^{-3}
30	20	10	1.29×10^{-1}	4.85×10^{-3}
40	20	0	8.24×10^{-2}	5.71×10^{-2}

Table 7.10: Neutron and photon dose rate calculated at 1.5 m from centre of source for a 60 cm thick iron/wax/iron spherical geometry, as function of iron/wax depth.

Chapter 8

REFERENCES

Amc94 "A Monte Carlo Code for Particle Transport," Los Alamos Science Number 22, Unpublished (1994).

Bak99 Baker S., Jones D. and Watkins K., "Anisotropic Integral Transport Solution in Arbitrary Three-dimensional Geometry", ANS Transactions, Boston, June 1999.

Ber63a Bertini H.W., Phys. Rev. **13** (1963)1801.

Ber63b Bertini H.W., *Low energy intranuclear cascsde calculation*, Phys. Rev. **131**, (1963)1801.

Ber65 Bertini H.W., Phys. Rev. **138** (1965)AB2.

Ber69 Bertini H.W., Phys. Rev. **188** (1963)1711.

Bla71 Blan M., *Hybrid model for pre-equilibrium decay in nuclear reactions.* Phys. Rev. Lett. **27**, (1971) 337.

Bla72 Blan M., *Importance of the nuclear density distribution in pre-equilibrium decay*, Phys. rev. Lett. **28**, (1972)757.

Bla75 Blan M., *Pre-equilibrium decay*, Ann. Rev. Nucl. Sci. textbf25, (1975)123.

Bot87 Botvina A.S., Iljinov A.S., Mashustin I.N., bondorf J.P., Donangelo R. and Sneppen, Nucl. Phys. **A475**, (1987)663.

Boz01 Bozkurt A., Chao T.C. and Xu X.G., Fluence-to-dose conversion coefficients based on the vip-man anatomic model and MCNPX code for monoenergetic neutrons above 20 MeV. *Healthy Phys.* Vol.**81** (2001)184.

Bri93 Briesmeister J. and Ed., "MCNP-A General Purpose Monte Carlo Code for Neutron and Photon Transport, Version 4A", LA-12625-M, Los Alamos National Laboratory (1993).

Bro83 Broome T.A., Perry D.R., Stapleton G.B. and Duc D., Particle distribution around a copper beam stop for 72 MeV protons. *Healthy Phys.* **44** (1983)487.

Cam03 Campbell J.M., Frankle S.C. and Little R.C., *A Continuous Energy Neutron Data Library Based on ENDF/B VI*, ENDF60 Release 6, **LA-UR-03-0954**, LANL.

CER05 http://wwwasd.web.cern.ch/wwwasd/geant4/geant4.html.

Cha01 Chao T.C., Bozkurt A. and Xu X.G., Conversion coefficients based on the vip-man anatomical model and EGS4-VLSI code for external monoenergetic photons from 10 keV to 10 MeV. *Healthy Phys.* Vol.**81** (2001)163.

Cug87 Cugnon J., Nucl. Phys. **A62** (1987)751.

Cug88 Cugnon J. and Lenaire M.C., Nucl. Phys. **A489** (1988)505.

Cug97 Cugnon J.,Volant C. and Vuillier S., Nucl. Phys. **A620** (1997)457.

Cul03 Cullen D.E., Hansen L.F., Lent E.M. and Plechaty E.F., *Thermal Scattering Law Data: Implementation and testing using the Monte Carlo transport codes COG, MCNP and TART.*, U.S. Department of Energy, UCRL-ID153656, 17 May 2003 and http://apollo.osti.gov/bridge/

END ENDF/B-VI Release 6, http://www.llnl.gov/cullenl/neutron.htm.

END60 http://www-rsicc.ornl.gov/codes/dlc/dlc2/dlc-200.htm.

Eng73 Engle W.W., Oak Ridge National Laboratory Report, ORNL/K-1693, (1967) updated 1973.

Fas01 Fasso A. *et al.*, FLUKA Status and prospective for hadronic applications, Proc. of the Monte Carlo 2000 Conf. Lisbon, October 2000, A. Kling et al Edn. Springer-Verlag Berlin (2001) 955.

Fer35 Phys. Rev., **48** (1935)265.

Fer97 Ferrari A., Pellicioni M. and Pillon M., *Fluence to effective dose conversion coefficiennts for neutrons, photons, electrons and protons up to 1000 MeV*, Radiat. Prot. Dosim., Vol. 69, No.2 (1997) 97.

Fes80 Feshbach H., Kerman A.K. and Koonin S., Statistical theory of multstep compound and direct reactions.*Ann. Phys.* 125 (1980)429.

Fes95 Feshbach H., Statistical multistep reactions. *Nuclear Physics News*, **5** (1995)17, and references therein.

Gri66 Griffin J.J., "Statistical Model of Intermediate Structure", Phys. Rev. Letters 17, 9, 1966.

Hod97 Hodgson P.E., Gadioli E. and Gadioli Erbra E., *Introductory Nuclear Physics.* Clarendon Press, Oxford, 1997.

Hub75 Hubbell J.H., Viegele W.J., Briggs E.A., Brown R.T., Cromer D.T. and Howerton R.J., *"Atomic form farctors, incoherent scattering functions and protons scattering cross section"*., J. Phys. Chem. Ref., (1975)471.

ICR84 *Stopping powers for electrons and positrons.* International Commission on Radiation Units and Measurements, ICRU Report **37**, Washington D.C. (1984).

Jan82 Janni J.F., *Proton range-energy table, 1 keV - 10 GeV.* At. Nucl. Data Tables **27** (1982)150.

Kon04 Koning A.J., Duijvestijn M.C., van der Marck S.C., Klein Meulekamp R. and Hogenbrik A., *New Nuclear Data Evaluations for Ca,Sc,Fe,Ge,Pb, and Bi.*, Proc. Intern. Conf. on Nuclear Data for Science and Technology, Santa Fe, New Mexico, USA, September 26 - October 1 2004 ed. AIP(2005).

Lan44 Landau L., *On the energy loss of fast particles by ionisation*, J. Phys., **8**, (1944)201.

Leo87 Leo W.R., *Techniques for Nuclear and Particle Physics Experiments.* Springer-Verlag, Berlin. (1987).

LLN89 Lawrence Livermore National Laboratory, Livermore, CA. Review 4, Part A: 1 to 50 and Part B:50 to 100, Vol. **60**. (1989).

Man24 MCNPX Manual version 2.4, http://mcnpx.lanl.gov/documents/

MCN05 MCNPX Beta Test Version 2.5.0, http://mcnpx.lanl.gov/

Mok98 Mokhov N.V. *et al.*, Mars code development, Proc. of the 4th Workshop on Simulating Accelerator Environments (SARE4) Knoxville TN, USA, Sept. 1998, Ed. T. Gabriel, ORNL (1998)87.

Nis88 Nishioka H.,Weidenmuller H.A. and Yoshida S., *Ann. Phys. (NY)* **183**, (1988)166.

Nor90 Nortier F.M., *Considerations Concerning Targetry for Radioisotope Production at the NAC and the production of gallium-67, indium-111, and cadmium-109.* Thesis: University of Stellenbosch, South Africa (1990).

Rho73 Rhoades W.A., *et al.*, Oak Ridge National Laboratory Report, ORNL/TM-4280 (1973).

Ros42 Rossi B. and Greisen K., *Cosmic-ray theory*, Rev. Mod. Phys. **13**, (1942)240.

RSI05 http://www-rsicc.ornl.gov/codes/ccc/ccc6/ccc-696.htm.

Ryd82 Ryder R., *Neutron production from proton and deuterons*, Daresbury Laboratory technical memorandum DL/NUC/TM 60A, Daresbury, UK (1982).

Sch01 Schneider U., Besserer J. and Pelmer P., *On small angle multiple Coulomb Scattering of protons in Gaussian approximation*, Z. Med. Phys., Vol. 11, **No.2** (2001)110.

Sel64 Seltzer S.M. and Berger M.J., *Energy loss straggling of protons and mesons* in Studies In Penetration of Charged Perticles in Matter, Nucl. Sc. Seies **39**, Nat. Ac. of Sc., Washington DC (1964).

Ser47 Serber R., Phys. Rev. **72**, (1947)1114.

Ste71 Sternheimer R.M. and Peierls R.F., *General expression for the density effect for the ionization loss of charged particles*, Phys. Rev. **B3** (1971)3681.

Ste82 Sternheimer R.M., Seltzer S.M. and Berger M.J., *Density effects for the ionization loss of charged particles in various*, Phys. Rev **B26** (1982)6067.

Ste90 Steyn G.F., *Bormbardment Facilities for Radioisotope Production at the NAC and the Production of iron-52, iron-55 and rubidium-81.* Thesis: University of Stellenbosch, South Africa (1990).

Ste92 Steyn G.F., van Rooyen T.J., Binns P.J., Hough J.H., Nortier F.M. and Mills S.J., *Design calculations for a local radiation shield of a radioisotope production target bombardment station*, Nucl. Instr. Meth. Phys. Rev., **A316** (1992)128.

Str70 Strom E. and Israel H.I., *"Proton cross section from 1keV to 100 MeV for elements Z=1 to Z=100"*., Nuclear Data Tables, Vol.**A7**, (1970)565.

Tam82 Tamura T., Udagawa T. and Lenske H., *Phys. Rev.* **C26** (1982)379.

Tay58 Phys. Rev., **110** (1958)1216.

Vav57 Vavilov P.V., *Ionisation losses of high energy heavy charged particles*, Soviety Phys., **JETP 5**, (1957)749.

Wal92 Waldeer K.T. and Urbassek H.M., *Small angle multiple scattering of light particles at a glancing incident for screened Coulomb interaction*, J. Phys. A: Math. Gen., **25** (1992)807.

Wil95 Williams M.L. and Asgari M., "Computation of Continuous-Energy Neutron Spectra With Discrete Ordinates Transport Theory," *Nucl. Sci. Engr.* **121** (1995)173.

Wil99 Williams M.L., Jones D.B. and Watkins K.E., "Trends in Deterministic Transport Code Development", *Trans. Am. Nucl. Soc.,* **80** (1999)152.

Zob68 Zobel W., Maienschein F.C., Todd J.H. and Chapman G.T., *Gamma rays from bombardment of light and intermediate weight nuclei by 16 to 160 MeV protons and 59 MeV alpha particles*, Nucl. Sc. Eng. **32**, (1968)392.